Transient effects in a double quantum dot sandwiched laterally between superconducting and metallic leads

R. Taranko,[1] K. Wrześniewski,[2] B. Baran,[1] I. Weymann,[2] and T. Domański[1]
[1]*Institute of Physics, M. Curie-Skłodowska University, 20-031 Lublin, Poland*
[2]*Institute of Spintronics and Quantum Information, Faculty of Physics, Adam Mickiewicz University, 61-614 Poznań, Poland*

(Received 9 September 2020; revised 24 March 2021; accepted 9 April 2021; published 29 April 2021)

We study the transient phenomena appearing in a subgap region of the double quantum dot coupled in series between the superconducting and normal metallic leads, focusing on the development of the superconducting proximity effect. For the uncorrelated nanostructure we derive explicit expressions of the time-dependent occupancies in both quantum dots, charge currents, and electron pairing induced on individual dots and between them. We show that the initial configurations substantially affect the dynamical processes, in which the in-gap bound states emerge upon coupling the double quantum dot to the superconducting reservoir. In particular, the superconducting proximity effect would be temporarily blocked whenever the quantum dots are initially singly occupied. Such *triplet/Andreev blockade* has been recently reported experimentally for double quantum dots embedded in the Josephson [Bouman *et al.*, Phys. Rev. B **102**, 220505 (2020)] and Andreev [Zhang *et al.*, arXiv:2102.03283 (2021)] junctions. We also address the role of correlation effects within the lowest-order decoupling scheme and by the time-dependent numerical renormalization group calculations. Competition of the repulsive Coulomb interactions with the superconducting proximity effect leads to renormalization of the in-gap quasiparticles, speeding up the quantum oscillations and narrowing a region of transient phenomena, whereas the dynamical Andreev blockade is well pronounced in the weak interdot coupling limit. We propose feasible methods for detecting the characteristic timescales that could be observable by the Andreev spectroscopy.

DOI: 10.1103/PhysRevB.103.165430

I. INTRODUCTION

The transport of charge [1] and energy [2] through heterostructures, where nanoscopic objects are attached to superconductor(s), is nowadays of great interest not only from the point of view of basic science but, most importantly, due to promising future applications. For instance, the quantum dots confined in a Y-shape junction between two conducting and one superconducting electrode can be a source of spatially entangled electrons from the dissociated Cooper pairs [3]. Another intensively studied field encompasses semiconducting nanowires and/or magnetic nanochains hybridized with bulk superconductors, where the emerging topological phase hosts Majorana quasiparticles, which are ideal candidates for stable qubits and could enable quantum computations owing to their non-Abelian character [4]. These and many similar phenomena stem from the presence of bound states that are induced at quantum dots/impurities [5], dimers [6], nanowires [7,8], and magnetic nanoislands [9] proximitized to bulk superconductors.

Since double quantum dot (DQD) configurations provide a versatile platform for the implementation of quantum information processing [10,11], such systems have also been considered in hybrid setups involving superconducting elements. Experimentally, their bound states have been probed by the tunneling spectroscopy, using InAs [12–17], InSb [18], Ge/Si [19] quantum dots or carbon nanotubes [20,21] contacted with superconducting lead(s), as well as by the scanning tunneling microscopy (STM) applied to the magnetic dimers deposited on superconducting substrates [6,22–24]. The single V, Cr, Mn, Fe, and Co atoms deposited on aluminum have revealed that Cr and Mn atoms have contributions from different orbitals to subgap quasiparticles, whereas the other elements merely consist of one pair of the in-gap bound states [25]. The properties of superconductor-proximitized double quantum dots (dimers) have been studied theoretically by a number of groups [18,26–47]. So far, however, hybrid DQD systems have been investigated mainly under the stationary conditions [5,31], while their transient behavior remains to a large extent unexplored.

In this paper we extend these studies by analyzing the dynamical phenomena after an abrupt attachment of a DQD to the normal (N) and superconducting (S) electrodes (Fig. 1). We examine the development of the electron pairings on individual quantum dots as well as between them and analyze a gradual buildup of the subgap bound states. Our analytical expressions (obtained for uncorrelated setups) and numerical results (in the presence of Coulomb interactions) show that the initial configurations substantially affect the dynamical superconducting proximity effect. In particular, we reveal that the leakage of Cooper pairs onto both quantum dots would be blocked whenever the dots are initially singly occupied by the same spin electrons. This *triplet/Andreev blockade* has been recently observed experimentally under the stationary conditions, using DQD in the Josephson (S-DQD-S) [16] and Andreev (N-DQD-S) junctions [17]. To get a deeper

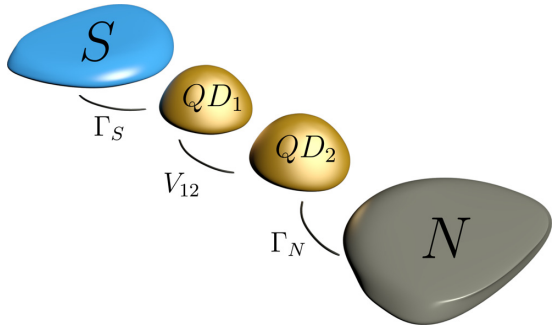

FIG. 1. Schematic view of the quantum dots ($QD_{1,2}$) embedded in series between the normal (N) and superconducting (S) leads with the couplings Γ_N and Γ_S, respectively.

insight into the dynamical behavior in the considered N-DQD-S setup, we analyze in detail various time-dependent quantities taking into account several initial configurations. To determine all relevant timescales and examine the role of initial conditions, we first derive the analytical results, neglecting the two-body interactions. We then take into account the effects of the Coulomb repulsion using two different techniques. To capture correlation effects, we make use of the mean-field approximation to the Coulomb interaction; however, in a further step we also employ the time-dependent numerical renormalization group (tNRG) method [48–50], which allows for obtaining very accurate predictions for the transient behavior of an unbiased junction. We demonstrate that the relevant timescales are revealed in the transient currents and could show up in other quench protocols, e.g., upon varying the quantum dot levels.

We believe that our study provides a valuable insight into the dynamical superconducting proximity effect and the evolution of in-gap quasiparticles toward their stationary state values in the case of double quantum dots. Our findings could be tested using the state of the art experimental techniques, in particular, the subgap (Andreev) spectroscopy, and we hope that this work will foster further efforts in studying dynamics of hybrid quantum dot structures. Finally, we would like to note that our analytical formalism can be extended to other quantum quench protocols, for example, due to abrupt change of the quantum dot energy levels or periodic driving. Moreover, it is also important to note that the presented analysis focuses on relatively weak coupling to the normal contact and as such it does not encompass the subgap Kondo physics [28,39]. This transport regime is definitely interesting and would require further analysis; however, it goes beyond the scope of the present work.

The paper is organized as follows. In Sec. II we introduce the microscopic model and describe the formalism for determination of time-dependent quantities. Section III presents the dynamics of the uncorrelated N-DQD-S setup, whereas Sec. IV is devoted to the studies of the role of the Coulomb interaction. In Sec. V we summarize the main results and give a brief outlook. The technical details concerning the equations of motion of the uncorrelated setup are presented in Appendix A. In Appendix B we provide the expressions for the charge currents, and Appendix C presents the analytical results for the uncorrelated DQD-S case.

II. FORMULATION OF THE PROBLEM

A. Microscopic model

The system under consideration (Fig. 1) consists of two quantum dots ($QD_{1,2}$) placed in linear configuration between the superconducting (S) and normal (N) leads. The Hamiltonian of this setup can be expressed as

$$\hat{H} = \hat{H}_N + \hat{H}_S + \hat{H}_{\rm hybr} + \sum_{j=1,2} \hat{H}_{{\rm QD}_j}, \tag{1}$$

where $\hat{H}_N = \sum_{\mathbf{k}} \varepsilon_{N\mathbf{k}\sigma} \hat{c}^\dagger_{N\mathbf{k}\sigma} \hat{c}_{N\mathbf{k}\sigma}$ describes the normal lead electrons and the bulk superconductor is treated in the BCS scenario:

$$\hat{H}_S = \sum_{\mathbf{q}\sigma} \varepsilon_{S\mathbf{q}} \hat{c}^\dagger_{S\mathbf{q}\sigma} \hat{c}_{S\mathbf{q}\sigma} - \sum_{\mathbf{q}} \left(\Delta \hat{c}^\dagger_{S\mathbf{q}\uparrow} \hat{c}^\dagger_{S-\mathbf{q}\downarrow} + {\rm H.c.} \right). \tag{2}$$

As usual, $\hat{c}_{\beta\mathbf{k}(\mathbf{q})\sigma}$ denote the second quantization operators of the normal ($\beta = {\rm N}$) and superconducting ($\beta = {\rm S}$) lead electrons, respectively. They are characterized by momenta $\mathbf{k}(\mathbf{q})$, energies $\varepsilon_{N\mathbf{k}(S\mathbf{q})}$, and spin $\sigma = \uparrow, \downarrow$. We assume the pairing potential Δ of superconducting lead to be real and restrict our considerations to the electronic states inside this pairing gap window.

The external leads are interconnected via the quantum dots $\hat{H}_{{\rm QD}_j} = \sum_\sigma \varepsilon_{j\sigma} \hat{c}^\dagger_{j\sigma} \hat{c}_{j\sigma}$ whose energies are denoted by $\varepsilon_{j\sigma}$. In our considerations we assume that the level spacing in the dots is much larger than other energy scales, such that only a single orbital level in each quantum dot is relevant for transport. The constituents of the considered setup are hybridized through

$$\hat{H}_{\rm hybr} = \sum_\sigma \Bigg(V_{12} \hat{c}^\dagger_{1\sigma} \hat{c}_{2\sigma} + \sum_{\mathbf{q}} V_{S\mathbf{q}} \hat{c}^\dagger_{S\mathbf{q}\sigma} \hat{c}_{1\sigma} + \sum_{\mathbf{k}} V_{N\mathbf{k}} \hat{c}^\dagger_{N\mathbf{k}\sigma} \hat{c}_{2\sigma} + {\rm H.c.} \Bigg), \tag{3}$$

where V_{12} denotes the interdot coupling, whereas $V_{S\mathbf{q}(N\mathbf{k})}$ describes the coupling of $QD_{1(2)}$ to the external S (N) electrode. For convenience, we introduce the auxiliary couplings $\Gamma_\beta = 2\pi \sum_{\mathbf{k}} |V_{\beta\mathbf{k}}|^2 \delta(\omega - \varepsilon_{\beta\mathbf{k}})$, assuming them to be constant. Such constraint is realistic in the subgap region, $|\omega| < \Delta$, that is of our interest here.

For analytical determination of the time-dependent quantities we shall treat the pairing gap Δ as the largest energy scale in this problem. Formally, we thus focus on the superconducting atomic limit $\Delta \to \infty$. To simplify our notation we set $\hbar = e = k_B = \Gamma_S = 1$ when energies, currents, and time are expressed in units of Γ_S, $e\Gamma_S/\hbar$, and $\hbar/\Gamma_S$, respectively. In realistic situations $\Gamma_S \sim 200$ μeV; therefore the typical time unit would be 3.3 psec and the current unit ~48 nA.

B. Transient evolution

For $t < 0$ we assume all parts of the considered system to be disconnected. The evolution of the charge occupancies of quantum dots, $n_{j\sigma}(t)$, the transient currents flowing from the leads, $j_{N(S)\sigma}(t)$, and the pairing correlation functions, $\langle \hat{c}_{j\downarrow}(t) \hat{c}_{j\uparrow}(t) \rangle$ and $\langle \hat{c}_{1\downarrow}(t) \hat{c}_{2\uparrow}(t) \rangle$, driven by an abrupt hybridization (3) at $t = 0$ will bring the information about

the superconducting proximity effect, giving rise to the emergence of subgap quasiparticles.

The expectation value $\langle\hat{O}\rangle$ of any observable $\hat{O}$ can be determined by solving the Heisenberg equation of motion $i\frac{d}{dt}\hat{O} = [\hat{O}, \hat{H}]$. For this purpose it is convenient to apply the Laplace transform

$$\hat{O}(s) = \int_0^\infty dt e^{-st}\hat{O}(t) \tag{4}$$

to incorporate the initial ($t = 0$) conditions [51,52]. For example, the time-dependent occupancy of the jth QD would be formally given by

$$n_{j\sigma}(t) = \langle \mathcal{L}^{-1}\{\hat{c}^\dagger_{j\sigma}(s)\}(t)\cdot\mathcal{L}^{-1}\{\hat{c}_{j\sigma}(s)\}(t)\rangle, \tag{5}$$

where $\mathcal{L}^{-1}\{\hat{c}^\dagger_{j\sigma}(s)\}(t)$ stands for the inverse Laplace transform of $\hat{c}^\dagger_{j\sigma}(s)$ and $\langle\cdots\rangle$ denotes the statistical averaging.

When neglecting the Coulomb interactions on both quantum dots, one can derive the explicit expressions for $\hat{c}^{(\dagger)}_{j\sigma}(s)$ and analytically determine the time-dependent expectation values of various observables (the influence of the correlation effects will be examined in Sec. IV). Let us now discuss the Laplace transforms of $\hat{c}_{j\sigma}(s)$, as they are crucial for the physical quantities of interest. Appendix A presents the Laplace-transformed Heisenberg equations (A1)–(A8) for arbitrary value of the pairing gap Δ. In the superconducting atomic limit ($\Delta\to\infty$) these equations simplify to

$$(s+i\varepsilon_{1\uparrow})\hat{c}_{1\uparrow}(s) = -i\frac{\Gamma_S}{2}\hat{c}^\dagger_{1\downarrow}(s) - iV_{12}\hat{c}_{2\uparrow}(s)+\hat{a}_1, \tag{6}$$

$$(s-i\varepsilon_{1\downarrow})\hat{c}^\dagger_{1\downarrow}(s) = -i\frac{\Gamma_S}{2}\hat{c}_{1\uparrow}(s) + iV_{12}\hat{c}^\dagger_{2\downarrow}(s)+\hat{a}_2, \tag{7}$$

$$\left(s+i\varepsilon_{2\uparrow}+\frac{\Gamma_N}{2}\right)\hat{c}_{2\uparrow}(s) = -iV_{12}\hat{c}_{1\uparrow}(s)+\hat{a}_3, \tag{8}$$

$$\left(s-i\varepsilon_{2\downarrow}+\frac{\Gamma_N}{2}\right)\hat{c}^\dagger_{2\downarrow}(s) = iV_{12}\hat{c}^\dagger_{1\downarrow}(s)+\hat{a}_4, \tag{9}$$

with $\hat{a}_j$ defined in (A13)–(A16). Here, we have used

$$\sum_{\mathbf{k}}\frac{|V_{N\mathbf{k}}|^2}{s\pm i\varepsilon_{N\mathbf{k}}} = \frac{\Gamma_N}{2\pi}\int_{-D}^{D}\frac{d\omega}{s\pm i\omega} = \frac{\Gamma_N}{\pi}\arctan\left(\frac{D}{|s|}\right),$$

which in the wide-bandwidth limit ($D\to\infty$) implies $\sum_{\mathbf{k}} V^2_{N\mathbf{k}}/(s\pm i\varepsilon_{N\mathbf{k}})\approx\Gamma_N/2$. In a similar way one finds

$$\sum_{\mathbf{q}}|V_{S\mathbf{q}}|^2\frac{s\pm i\varepsilon_{S\mathbf{q}}}{s^2+\varepsilon^2_{S\mathbf{q}}+\Delta^2}\approx\frac{\Gamma_S}{2}\frac{s}{\sqrt{s^2+\Delta^2}},$$

$$\sum_{\mathbf{q}}|V_{S\mathbf{q}}|^2\frac{\Delta}{s^2+\varepsilon^2_{S\mathbf{q}}+\Delta^2}\approx\frac{\Gamma_S}{2}\frac{\Delta}{\sqrt{s^2+\Delta^2}}.$$

Thus, in the superconducting atomic limit we have $\lim_{\Delta\to\infty}\sum_{\mathbf{q}}|V_{S\mathbf{q}}|^2(s\pm i\varepsilon_{S\mathbf{q}})/(s^2+\varepsilon^2_{S\mathbf{q}}+\Delta^2)\approx 0$ and $\lim_{\Delta\to\infty}\sum_{\mathbf{q}}|V_{S\mathbf{q}}|^2\Delta/(s^2+\varepsilon^2_{S\mathbf{q}}+\Delta^2)\approx\Gamma_S/2$, respectively.

For the specific case of $\varepsilon_{j\sigma}=0$, the Laplace transforms of QD operators can be expressed as

$$\begin{aligned}
\hat{c}_{1\uparrow/\downarrow}(s) = {}& \hat{c}_{1\uparrow/\downarrow}(0)\frac{u(s)(s+\Gamma_N/2)}{W(s)} - \hat{c}_{2\uparrow/\downarrow}(0)\frac{iV_{12}u(s)}{W(s)} \mp \hat{c}^\dagger_{1\downarrow/\uparrow}(0)\frac{\Gamma_S(s+\Gamma_N/2)^2}{2W(s)} \pm \hat{c}^\dagger_{2\downarrow/\uparrow}(0)\frac{\Gamma_S(s+\Gamma_N/2)V_{12}}{2W(s)} \\
& - \sum_{\mathbf{k}}\left[\hat{c}_{N\mathbf{k}\uparrow/\downarrow}(0)\frac{V_{N\mathbf{k}}}{s+i\varepsilon_{N\mathbf{k}}}\frac{V_{12}u(s)}{W(s)} \mp \hat{c}^\dagger_{N\mathbf{k}\downarrow/\uparrow}(0)\frac{V_{N\mathbf{k}}}{s-i\varepsilon_{N\mathbf{k}}}\frac{i\Gamma_S V_{12}(s+\Gamma_N/2)}{2W(s)}\right] \\
& - \frac{i\Gamma_S}{2W(s)}\sum_{\mathbf{q}}\left[\frac{V_{S\mathbf{q}}\Delta u(s)}{s^2+\varepsilon^2_{S\mathbf{q}}+\Delta^2}\hat{c}_{S-\mathbf{q}\uparrow/\downarrow}(0) \pm i\frac{V_{S\mathbf{q}}u(s)(s+i\varepsilon_{S\mathbf{q}})}{s^2+\varepsilon^2_{S\mathbf{q}}+\Delta^2}\hat{c}^\dagger_{S\mathbf{q}\downarrow/\uparrow}(0)\right] \\
& + \frac{u(s)(s+\Gamma_N/2)}{W(s)}\left[\mp\sum_{\mathbf{q}}\frac{V_{S\mathbf{q}}\Delta}{s^2+\varepsilon^2_{S\mathbf{q}}+\Delta^2}\hat{c}^\dagger_{S-\mathbf{q}\downarrow/\uparrow}(0) - i\sum_{\mathbf{q}}\frac{V_{S\mathbf{q}}(s-i\varepsilon_{S\mathbf{q}})}{s^2+\varepsilon^2_{S\mathbf{q}}+\Delta^2}\hat{c}_{S\mathbf{q}\uparrow/\downarrow}(0)\right],
\end{aligned} \tag{10}$$

$$\begin{aligned}
\hat{c}_{2\uparrow/\downarrow}(s) = {}& -\hat{c}_{1\uparrow/\downarrow}(0)\frac{iV_{12}u(s)}{W(s)} + \hat{c}_{2\uparrow/\downarrow}(0)\frac{1-V^2_{12}u(s)/W(s)}{s+\Gamma_N/2} \mp \hat{c}^\dagger_{1\downarrow/\uparrow}(0)\frac{V_{12}\Gamma_S(s+\Gamma_N/2)}{2W(s)} \mp \hat{c}^\dagger_{2\downarrow/\uparrow}(0)\frac{iV^2_{12}\Gamma_S}{2W(s)} \\
& + \sum_{\mathbf{k}}\left[\hat{c}_{N\mathbf{k}\uparrow/\downarrow}(0)\frac{V_{N\mathbf{k}}}{s+i\varepsilon_{N\mathbf{k}}}\frac{V^2_{12}u(s)/W(s)-1}{s+\Gamma_N/2} \pm \hat{c}^\dagger_{N\mathbf{k}\downarrow/\uparrow}(0)\frac{V_{N\mathbf{k}}}{s-i\varepsilon_{N\mathbf{k}}}\frac{V^2_{12}\Gamma_S}{2W(s)}\right] \\
& - \frac{V_{12}\Gamma_S(s+\Gamma_N/2)}{2W(s)}\left[\sum_{\mathbf{q}}\frac{V_{S\mathbf{q}}\Delta}{s^2+\varepsilon^2_{S\mathbf{q}}+\Delta^2}\hat{c}_{S-\mathbf{q}\uparrow/\downarrow}(0) \pm i\sum_{\mathbf{q}}\frac{V_{S\mathbf{q}}(s+i\varepsilon_{S\mathbf{q}})}{s^2+\varepsilon^2_{S\mathbf{q}}+\Delta^2}\hat{c}^\dagger_{S\mathbf{q}\downarrow/\uparrow}(0)\right] \\
& - \frac{iV_{12}u(s)}{W(s)}\left[\mp\sum_{\mathbf{q}}\frac{V_{S\mathbf{q}}\Delta}{s^2+\varepsilon^2_{S\mathbf{q}}+\Delta^2}\hat{c}^\dagger_{S-\mathbf{q}\downarrow/\uparrow}(0) - i\sum_{\mathbf{q}}\frac{V_{S\mathbf{q}}(s-i\varepsilon_{S\mathbf{q}})}{s^2+\varepsilon^2_{S\mathbf{q}}+\Delta^2}\hat{c}_{S\mathbf{q}\uparrow/\downarrow}(0)\right],
\end{aligned} \tag{11}$$

where

$$u(s) = s(s + \Gamma_N/2) + V_{12}^2, \tag{12}$$

$$W(s) = u^2(s) + \left(\frac{\Gamma_S}{2}\right)^2 \left(s + \frac{\Gamma_N}{2}\right)^2. \tag{13}$$

In Eqs. (10) and (11) there appears the pairing gap Δ, originating from the auxiliary operators $\hat{a}_j$. We impose the superconducting atomic limit values later on, when computing the statistically averaged observables [51].

The 4th-order polynomial (13) can be rewritten as $W(s) = s^4 + b_3 s^3 + b_2 s^2 + b_1 s + b_0$, with the real coefficients, $b_0 = V_{12}^4 + \Gamma_S^2\Gamma_N^2/16$, $b_1 = \Gamma_N V_{12}^2 + \Gamma_N\Gamma_S^2/4$, $b_2 = 2V_{12}^2 + (\Gamma_S^2 + \Gamma_N^2)/4$, and $b_3 = \Gamma_N$. It can be recast into a product $W(s) = (s - s_1)(s - s_2)(s - s_3)(s - s_4)$, whose roots obey $s_2 = s_1^*$ and $s_3 = s_4^*$. Their knowledge enables us to obtain the inverse Laplace transforms of $\hat{c}_{j\sigma}(s)$ operators, expressing the time-dependent charge occupancies $n_{j\sigma}(t)$, pairing correlation functions, $\langle \hat{c}_{j-\sigma}(t)\hat{c}_{j\sigma}(t)\rangle$, $\langle \hat{c}_{1\downarrow}(t)\hat{c}_{2\uparrow}(t)\rangle$, and transient currents induced between various sectors of the N-DQD-S setup.

III. DYNAMICS OF UNCORRELATED SETUP

In this section we analyze the time-dependent observables obtained analytically for N-DQD-S nanostructure by the equation of motion procedure in the absence of the Coulomb repulsion. We begin by discussing the electron occupancies of each QD derived by inserting the inverse Laplace transforms [Eqs. (10) and (11)] to Eq. (5). For $t < 0$, all parts of the setup are disconnected; therefore the occupancy $n_{j\sigma}(t > 0)$ consists of the contributions from the initial expectation values of $n_{j\sigma}(0)$, $\langle \hat{c}^\dagger_{N\mathbf{k}\sigma}(0)\hat{c}_{N\mathbf{k}\sigma}(0)\rangle$, $\langle \hat{c}^\dagger_{S\mathbf{q}\sigma}(0)\hat{c}_{S\mathbf{q}\sigma}(0)\rangle$, and $\langle \hat{c}^{(\dagger)}_{S\mathbf{q}\sigma}(0)\hat{c}^{(\dagger)}_{S-\mathbf{q}\bar{\sigma}}(0)\rangle$, where $\bar{\sigma}$ is opposite spin to σ. In the superconducting atomic limit, for $t > 0$, we obtain

$$\begin{aligned} n_{1\uparrow/\downarrow}(t) = {} & n_{1\uparrow/\downarrow}(0)\left(\mathcal{L}^{-1}\left\{\frac{u(s)(s+\Gamma_N/2)}{W(s)}\right\}(t)\right)^2 + n_{2\uparrow/\downarrow}(0)V_{12}^2\left(\mathcal{L}^{-1}\left\{\frac{u(s)}{W(s)}\right\}(t)\right)^2 \\ & + [1 - n_{1\downarrow/\uparrow}(0)]\Gamma_S^2/4\left(\mathcal{L}^{-1}\left\{\frac{(s+\Gamma_N/2)^2}{W(s)}\right\}(t)\right)^2 + [1 - n_{2\downarrow/\uparrow}(0)]V_{12}^2\Gamma_S^2/4\left(\mathcal{L}^{-1}\left\{\frac{s+\Gamma_N/2}{W(s)}\right\}(t)\right)^2 \\ & + V_{12}^2\frac{\Gamma_N}{2\pi}\int_{-\infty}^{\infty} d\varepsilon f_N(\varepsilon)\mathcal{L}^{-1}\left\{\frac{u(s)}{(s+i\varepsilon)W(s)}\right\}(t)\cdot\mathcal{L}^{-1}\left\{\frac{u(s)}{(s-i\varepsilon)W(s)}\right\}(t) \\ & + \Gamma_N\Gamma_S^2V_{12}^2/8\pi\int_{-\infty}^{\infty} d\varepsilon[1 - f_N(\varepsilon)]\mathcal{L}^{-1}\left\{\frac{s+\Gamma_N/2}{(s+i\varepsilon)W(s)}\right\}(t)\cdot\mathcal{L}^{-1}\left\{\frac{s+\Gamma_N/2}{(s-i\varepsilon)W(s)}\right\}(t), \end{aligned} \tag{14}$$

$$\begin{aligned} n_{2\uparrow/\downarrow}(t) = {} & n_{1\uparrow/\downarrow}(0)V_{12}^2\left(\mathcal{L}^{-1}\left\{\frac{u(s)}{W(s)}\right\}(t)\right)^2 + n_{2\uparrow/\downarrow}(0)\left(\mathcal{L}^{-1}\left\{\frac{1}{s+\Gamma_N/2} - \frac{u(s)V_{12}^2}{W(s)(s+\Gamma_N/2)}\right\}(t)\right)^2 \\ & + [1 - n_{1\downarrow/\uparrow}(0)]V_{12}^2\Gamma_S^2/4\left(\mathcal{L}^{-1}\left\{\frac{s+\Gamma_N/2}{W(s)}\right\}(t)\right)^2 + [1 - n_{2\downarrow/\uparrow}(0)]V_{12}^4\Gamma_S^2/4\left(\mathcal{L}^{-1}\left\{\frac{1}{W(s)}\right\}(t)\right)^2 \\ & + \frac{\Gamma_N}{2\pi}\int_{-\infty}^{\infty} d\varepsilon f_N(\varepsilon)\mathcal{L}^{-1}\left\{\left(\frac{V_{12}^2u(s)}{W(s)} - 1\right)\frac{1}{(s-i\varepsilon)(s+\Gamma_N/2)}\right\}(t)\cdot\mathcal{L}^{-1}\left\{\left(\frac{V_{12}^2u(s)}{W(s)} - 1\right)\left(\frac{1}{(s+i\varepsilon)(s+\Gamma_N/2)}\right)\right\}(t) \\ & + \Gamma_N\Gamma_S^2V_{12}^4/8\pi\int_{-\infty}^{\infty} d\varepsilon[1 - f_N(\varepsilon)]\mathcal{L}^{-1}\left\{\frac{1}{(s+i\varepsilon)W(s)}\right\}(t)\cdot\mathcal{L}^{-1}\left\{\frac{1}{(s-i\varepsilon)W(s)}\right\}(t), \end{aligned} \tag{15}$$

where $f_N(\varepsilon) = [1 + \exp(\varepsilon/k_BT)]^{-1}$. The time-dependent occupancies depend on the initial DQD configurations $n_j(0)$ [through the first four terms appearing in Eqs. (14) and (15)] and on the couplings to external leads (via the last two terms). Let us notice that for the initial triplet configuration $[n_{j\uparrow}(0) = 0,\ n_{j\downarrow}(0) = 1]$ the evolution of $n_{j\sigma}(t)$ would be solely controlled by the coupling Γ_N to the metallic lead.

As an example, in Fig. 2 we show the time-dependent occupancy of the second dot $n_{2\uparrow}(t)$ obtained for a strong interdot coupling $V_{12} = 4\Gamma_S$ in the unbiased heterostructure ($\mu_N = 0 = \mu_S$), assuming that initially only a spin-$\uparrow$ electron occupies the first QD, $(\mathrm{QD}_1, \mathrm{QD}_2) = (\uparrow, 0)$. For comparison, in the bottom panel we display the results in the absence of the metallic lead. We also present the contributions described by the first four terms of the general formula Eq. (15), which are dependent on the initial occupancies. We can notice the oscillating character of $n_{2\uparrow}(t)$ with a damping imposed by Γ_N. The stationary limit value $n_{2\uparrow}(t \to \infty) = 0.5$ is approached through a sequence of quantum oscillations whose amplitude is exponentially suppressed with an envelope function $\exp(-\Gamma_N t/2)$. Such behavior is a consequence of the superposition of damped transient oscillations and another part which is independent of the initial occupancies [expressed by the last two terms in Eq. (15)] arising from the direct coupling of QD_2 to the normal lead. In the case of an unbiased junction, the

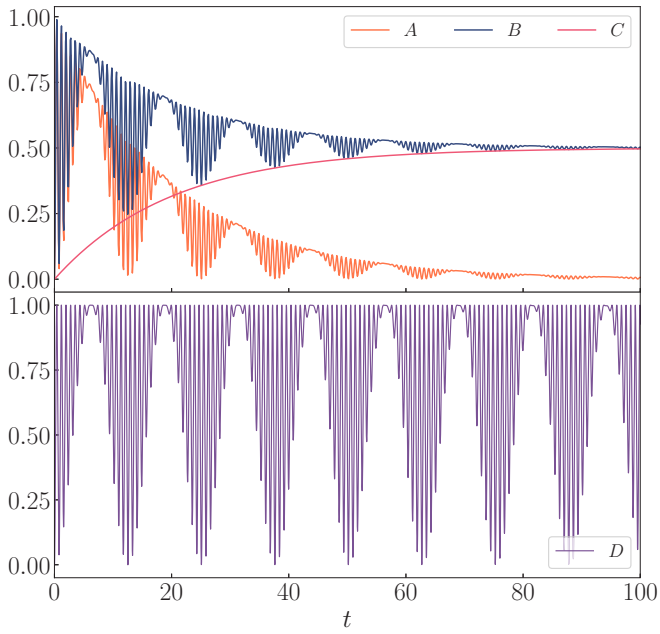

FIG. 2. Comparison of $n_{2\uparrow}(t)$ obtained for $\Gamma_N = 0.1\Gamma_S$ (curve B) with the case $\Gamma_N = 0$ (curve D). The curve C shows the contribution to $n_{2\uparrow}(t)$ due to the coupling Γ_N and the curve A refers to the contribution strictly dependent on the initial occupancies. Calculations have been done for $V_{12} = 4\Gamma_S$, assuming the initial conditions $(\mathrm{QD}_1, \mathrm{QD}_2) = (\uparrow, 0)$, $\Gamma_S = 1.0$, $\Gamma_N = 0.1$, $\varepsilon_{j\sigma} = 0$.

latter part simplifies to $\frac{1}{2}[1 - \exp(\Gamma_N t/2)]$, as displayed by the C curve in Fig. 2.

We now consider the subgap (Andreev) current $j_{N\sigma}(t)$, flowing from the normal lead to QD_2:

$$j_{N\sigma}(t) = 2\mathrm{Im}\sum_{\mathbf{k}} V_{N\mathbf{k}}\langle \hat{c}^{\dagger}_{2\sigma}(t)\hat{c}_{N\mathbf{k}\sigma}(t)\rangle. \tag{16}$$

In the wide-bandwidth limit it can be expressed as [51]

$$j_{N\sigma}(t) = 2\mathrm{Im}\sum_{\mathbf{k}} V_{N\mathbf{k}} e^{-i\varepsilon_{N\mathbf{k}}t}\langle \hat{c}^{\dagger}_{2\sigma}(t)\hat{c}_{N\mathbf{k}\sigma}(0)\rangle - \Gamma_N n_{2\sigma}(t). \tag{17}$$

Using the Hermitian conjugate of the operator $\hat{c}_{2\sigma}(t)$ presented in Eq. (11), we explicitly obtain

$$j_{N\sigma}(t) = -\Gamma_N n_{2\sigma}(t) + \frac{\Gamma_N}{\pi}\mathrm{Re}\left\{\int_{-\infty}^{\infty} d\varepsilon f_N(\varepsilon) e^{-i\varepsilon t} \times \left[\mathcal{L}^{-1}\left\{\frac{1}{(s - i\varepsilon)(s + g_n)}\right\}(t) - \mathcal{L}^{-1}\left\{\frac{u(s)V_{12}^2}{(s - i\varepsilon)(s + g_n)W(s)}\right\}(t)\right]\right\}, \tag{18}$$

where the time-dependent occupation $n_{2\sigma}(t)$ is given by Eq. (15).

Figure 3 displays the Andreev current $j_{N\uparrow}(t)$ computed for representative initial configurations, namely, A = (0, 0), B = (0, ↑), C = (↑↓, 0), and D = (↑, ↓). The quantum oscillations appearing in $j_{N\uparrow}(t)$ are identical with the time-dependent variation of the occupancies $n_{j\uparrow}(t)$ of the simpler DQD-S case (see Fig. 8 in Appendix C) and the supercurrent

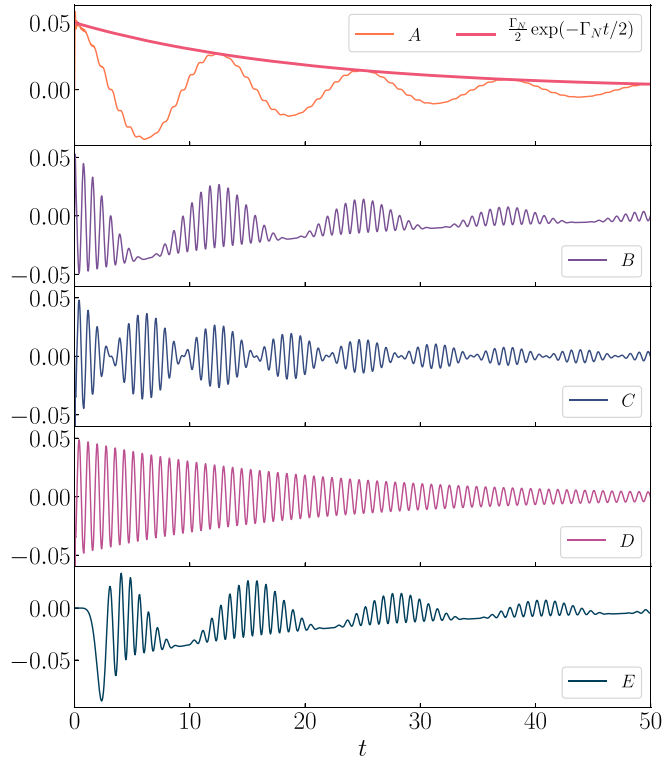

FIG. 3. The time-dependent current $j_{N\uparrow}(t)$ obtained for several initial configurations A = (0, 0), B = (0, ↑), C = (↑↓, 0), and D = (↑, ↓). The thick solid line shows the envelope function $\frac{\Gamma_N}{2}\exp(-\Gamma_N t/2)$, which refers to the damped currents obtained for all initial configurations. The bottom curve shows the current obtained for a finite interval of the switching time (see the text) of couplings between various constituents of the system, which can be compared with the curve B. Numerical results are obtained for $V_{12} = 4\Gamma_S$, $\Gamma_N = 0.1\Gamma_S$, and $\varepsilon_{j\sigma} = 0$.

$j_{S\sigma}(t)$ (Fig. 10). Here the main difference refers to the relaxation processes, which impose a damping on such quantum oscillations. This effect can be described by the envelope function $\frac{\Gamma_N}{2}\exp(-\Gamma_N t/2)$ (see Fig. 3). Apart from this damping, all other features appearing in $n_{j\sigma}(t)$ and $j_{S\sigma}(t)$ (e.g., oscillations with the periods of π/V_{12} and $4\pi/\Gamma_S$) are present in the time-dependent Andreev current $j_{N\sigma}(t)$, too.

Let us now comment on the large value of the transient current $j_{N\sigma}(0^+)$ right after forming the N-DQD-S setup (Fig. 3). Such rapid increase of the current from zero to $\frac{\Gamma_N}{2}$ is unphysical and in realistic experimental situations would not occur [53]. We have checked numerically that this artifact is absent for the smooth in time coupling protocol, $V_{N\mathbf{k}/S\mathbf{q}}(t) = \frac{V_{N\mathbf{k}/S\mathbf{q}}}{2}\{\sin[\pi(\frac{t}{t^*} - \frac{1}{2})] + 1\}$ for $0 < t \leqslant t^*$, and next imposing the constant value $V_{N\mathbf{k}/S\mathbf{q}}(t > t^*) = V_{N\mathbf{k}/S\mathbf{q}}$. The bottom (E) panel of Fig. 3 presents the transient current obtained for $t^* = 5$. Indeed, the absolute value of $|j_{N\uparrow}(t)|$ continuously increases from zero. Its variation in time in the region of $t \geqslant t^*$ is roughly the same as for the abrupt switching of coupling. A similar tendency holds for other quantities as well.

Using the expression (18) for $j_{N\sigma}(t)$ we define its time-dependent differential conductance $G_\sigma(\mu, t) = \frac{d}{d\mu} j_{N\sigma}(t)$ as a

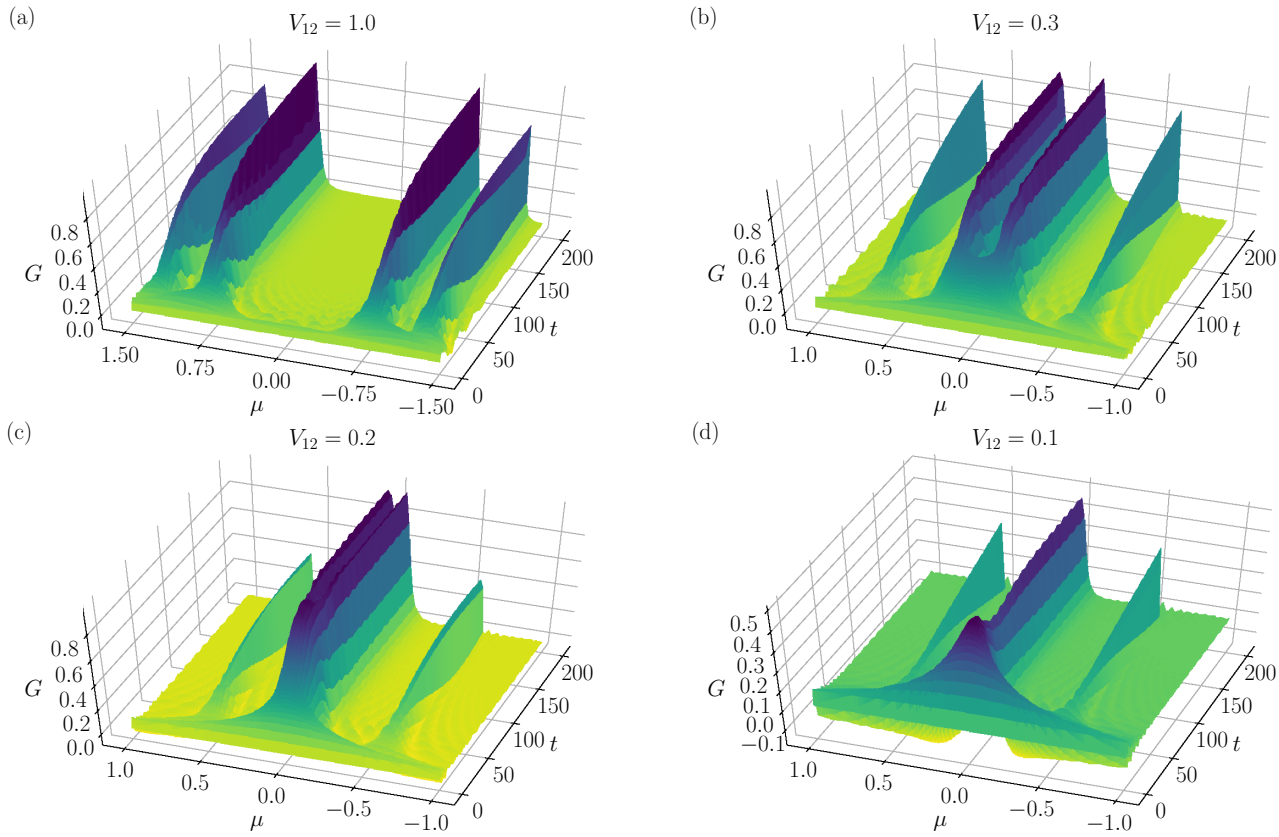

FIG. 4. The differential conductance G (in units of $2e^2/h$) as a function of time t and the bias voltage μ obtained for $V_{12} = 1$, 0.3, 0.2, and 0.1 [panels (a)–(d), respectively], assuming $\Gamma_S = 1$, $\Gamma_N = 0.1$, and $\varepsilon_{j\sigma} = 0$.

function of the bias voltage $\mu \equiv \mu_N - \mu_S$. At zero temperature it takes the following form (in units of $2e^2/h$):

$$G_\sigma(\mu,t) = \Gamma_N \mathrm{Re}\left\{\exp(-i\mu t)\left[\mathcal{L}^{-1}\left\{\frac{1}{(s-i\mu)(s+g_n)}\right\}(t) - V_{12}^2\mathcal{L}^{-1}\left\{\frac{u(s)}{(s-i\mu)(s+g_n)W(s)}\right\}(t)\right]\right.$$
$$\left. - \frac{\Gamma_N^2}{2}\left|\mathcal{L}^{-1}\left\{\frac{1}{(s+i\mu)(s+g_n)}\right\}(t) - V_{12}^2\mathcal{L}^{-1}\left\{\frac{u(s)}{(s+i\mu)(s+g_n)W(s)}\right\}(t)\right|^2 + \frac{\Gamma_N^2\Gamma_S^2V_{12}^4}{8}\left|\mathcal{L}^{-1}\left\{\frac{1}{(s+i\mu)W(s)}\right\}\right|^2\right\}. \tag{19}$$

Note that for the specific case of $\varepsilon_{j\sigma} = 0$, the differential conductance is spin-independent, $G_\sigma(\mu,t) = G(\mu,t)$.

The peaks appearing in the conductance $G(\mu,t)$ as a function of μ can be identified as the quasiparticle excitation energies between eigenstates comprising the even and odd numbers of electrons. For the uncorrelated DQD these bound states occur at $E_A = \pm\frac{1}{2}(\sqrt{4V_{12}^2 + \Gamma_S^2/4} \pm \frac{\Gamma_S}{2})$. We have calculated numerically the conductance (19) and observed the emergence of such bound states at E_A upon approaching the steady limit $t \to \infty$. In our N-DQD-S heterostructure they acquire a broadening (i.e., finite lifetime) due to scattering on a continuous spectrum of the normal lead. Electronic states from outside the pairing gap of superconducting lead could additionally broaden these bound states, supporting the relaxation mechanism [54].

In Fig. 4 we plot the differential conductance vs time and bias voltage for several interdot couplings, V_{12}, ranging from the large [panel (a)] to small [panel (d)] values. For $V_{12} \gtrsim \Gamma_S$, we observe the emergence of two broad structures at early times around the quasiparticle energies $\pm V_{12}$. In a short time period Δt right after the quench (here $\Delta t \sim 10$), these features evolve into distinct peaks, separated by $\sim\Gamma_S/2$. By decreasing V_{12}, we observe that the low-energy excitations are merged until a certain time after quench, whereas the higher-energy excitations are well separated from each other. With further decrease of V_{12} the energy difference between the low-energy excitations disappears. For very small $V_{12} = 0.1\Gamma_S$ [see Fig. 4(d)], the low-energy excitations form a single broad peak at zero energy, coexisting with the side-attached excitations at energies $\pm\Gamma_S/2$ of low intensity. This structure emerges at late times ($\sim$60) after the quench.

Finally, we examine the relationship between the excitation energies obtained from the differential conductance and the time-dependent electron pairings induced on individual quantum dots, $\langle \hat{c}_{j\downarrow}(t)\hat{c}_{j\uparrow}(t)\rangle$, and between them, $\langle \hat{c}_{1\downarrow}(t)\hat{c}_{2\uparrow}(t)\rangle$. Using the inverse Laplace transforms of the operators $\hat{c}_{j\sigma}(s)$ we get

$$\begin{aligned}\langle \hat{c}_{1\downarrow}(t)\hat{c}_{1\uparrow}(t)\rangle = i\Gamma_S/2\Bigg[&[n_{1\uparrow}(0)+n_{1\downarrow}(0)-1]\mathcal{L}^{-1}\left\{\frac{(s+\Gamma_N/2)^2}{W(s)}\right\}(t)\cdot\mathcal{L}^{-1}\left\{\frac{u(s)(s+\Gamma_N/2)}{W(s)}\right\}(t)\\ &+V_{12}^2[n_{2\uparrow}(0)+n_{2\downarrow}(0)-1]\mathcal{L}^{-1}\left\{\frac{s+\Gamma_N/2}{W(s)}\right\}(t)\cdot\mathcal{L}^{-1}\left\{\frac{u(s)}{W(s)}\right\}(t)\\ &-\frac{\Gamma_N V_{12}^2}{2\pi}\int_{-\infty}^{\infty}d\varepsilon[1-2f_N(\varepsilon)]\mathcal{L}^{-1}\left\{\frac{u(s)}{(s+i\varepsilon)W(s)}\right\}(t)\cdot\mathcal{L}^{-1}\left\{\frac{s+\Gamma_N/2}{(s-i\varepsilon)W(s)}\right\}(t)\Bigg],\end{aligned} \tag{20}$$

$$\begin{aligned}\langle \hat{c}_{2\downarrow}(t)\hat{c}_{2\uparrow}(t)\rangle = iV_{12}^2\frac{\Gamma_S}{2}\Bigg[&[1-n_{1\uparrow}(0)-n_{2\uparrow}(0)]\mathcal{L}^{-1}\left\{\frac{u(s)}{W(s)}\right\}(t)\cdot\mathcal{L}^{-1}\left\{\frac{s+\Gamma_N/2}{W(s)}\right\}(t)\\ &+\left[1-\sum_\sigma n_{2\sigma}(0)\right]\mathcal{L}^{-1}\left\{\frac{1}{W(s)}\right\}(t)\cdot\ \mathcal{L}^{-1}\left\{\frac{u(s)V_{12}^2}{W(s)(s+\Gamma_N/2)}-\frac{1}{s+\Gamma_N/2}\right\}(t)+\frac{\Gamma_N}{2\pi}\int_{-\infty}^{\infty}d\varepsilon[1-2f_N(\varepsilon)]\\ &\cdot\mathcal{L}^{-1}\left\{\frac{V_{12}^2u(s)}{(s+i\varepsilon)(s+\Gamma_N/2)W(s)}-\frac{1}{(s+i\varepsilon)(s+\Gamma_N/2)}\right\}(t)\cdot\mathcal{L}^{-1}\left\{\frac{1}{(s-i\varepsilon)W(s)}\right\}(t)\Bigg],\end{aligned} \tag{21}$$

$$\begin{aligned}\langle \hat{c}_{1\downarrow}(t)\hat{c}_{2\uparrow}(t)\rangle = V_{12}\frac{\Gamma_S}{2}\Bigg[&n_{1\uparrow}(0)\mathcal{L}^{-1}\left\{\frac{(s+\Gamma_N/2)^2}{W(s)}\right\}(t)\cdot\mathcal{L}^{-1}\left\{\frac{u(s)}{W(s)}\right\}(t)+n_{2\uparrow}(0)\mathcal{L}^{-1}\left\{\frac{s+\Gamma_N/2}{W(s)}\right\}(t)\\ &\cdot\mathcal{L}^{-1}\left\{\frac{V_{12}^2u(s)}{(s+\Gamma_N/2)W(s)}-\frac{1}{(s+\Gamma_N/2)}\right\}(t)-[1-n_{1\downarrow}(0)]\mathcal{L}^{-1}\left\{\frac{(s+\Gamma_N/2)u(s)}{W(s)}\right\}(t)\cdot\mathcal{L}^{-1}\left\{\frac{s+\Gamma_N/2}{W(s)}\right\}(t)\\ &-V_{12}^2[1-n_{2\downarrow}(0)]\mathcal{L}^{-1}\left\{\frac{u(s)}{W(s)}\right\}(t)\cdot\mathcal{L}^{-1}\left\{\frac{1}{W(s)}\right\}(t)-\frac{\Gamma_N V_{12}^2}{2\pi}\int_{-\infty}^{\infty}d\varepsilon[1-f_N(\varepsilon)]\mathcal{L}^{-1}\left\{\frac{u(s)}{(s+i\varepsilon)W(s)}\right\}(t)\\ &\cdot\mathcal{L}^{-1}\left\{\frac{1}{(s-i\varepsilon)W(s)}\right\}(t)+\frac{\Gamma_N}{2\pi}\int_{-\infty}^{\infty}d\varepsilon f_N(\varepsilon)\mathcal{L}^{-1}\left\{\frac{s+\Gamma_N}{(s-i\varepsilon)W(s)}\right\}(t)\\ &\cdot\mathcal{L}^{-1}\left\{\frac{V_{12}^2u(s)}{(s+i\varepsilon)(s+\Gamma_N/2)W(s)}-\frac{1}{(s+i\varepsilon)(s+\Gamma_N/2)}\right\}(t)\Bigg],\end{aligned} \tag{22}$$

with the auxiliary function $u(s)$ and $W(s)$ defined in Eqs. (12) and (13). For the DQD-S case, $\Gamma_N = 0$ (Appendix C), the nonvanishing values refer only to the imaginary (real) part of the on-dot $i = j$ (interdot $i \neq j$) pairings. The additional coupling of QD_2 to the normal lead allows the system to relax, evolving to its asymptotic (stationary) limit through a series of damped quantum oscillations. In consequence, the oscillating imaginary parts of $\langle \hat{c}_{j\downarrow}(t)\hat{c}_{j\uparrow}(t)\rangle$ and the real part of $\langle \hat{c}_{1\downarrow}(t)\hat{c}_{2\uparrow}(t)\rangle$ are now bounded between the curves $\pm\frac{\Gamma_S}{2}\exp(-\Gamma_N t/2)$ and $\pm\frac{\Gamma_S}{4}\exp(-\Gamma_N t/2)$. In contrast to the case of $\Gamma_N = 0$, the real parts of both on-dot pairing functions are finite and they smoothly evolve from zero to their steady limit values. A similar tendency can be observed for the imaginary part of the interdot pairing function, whose asymptotic value is rather residual.

Figure 5 shows the real part of $\langle \hat{c}_{1\downarrow}(t)\hat{c}_{1\uparrow}(t)\rangle$ with respect to time and bias voltage (top panel), compared with the asymptotics of the real parts of $\lim_{t\to\infty}\langle \hat{c}_{1/2\downarrow}(t)\hat{c}_{1/2\uparrow}(t)\rangle$, the imaginary part of $\lim_{t\to\infty}\langle \hat{c}_{1\downarrow}(t)\hat{c}_{2\uparrow}(t)\rangle$ (middle panel), and the differential conductance (bottom panel). We can notice a coincidence between the positions of the excitation energies appearing in the differential conductance (bottom panel) with the characteristic features manifested in the pairing functions. Namely, the real parts of the on-dot pairing functions (which are strongly energy-dependent) have the inflexion points exactly at quasiparticle energies of the in-gap bound states (top and middle panels). On the other hand, the imaginary part of the interdot pairing function exhibits a jump of its derivative $\frac{\partial}{\partial\mu}\langle \hat{c}_{1\downarrow}(t)\hat{c}_{2\uparrow}(t)\rangle$ from the positive (negative) to negative (positive) values. It occurs exactly at bias voltages equal to the bound state energies. Formally, these characteristic features originate from common poles of the diagonal and off-diagonal parts of the Green's function in the particle-hole (Nambu) representation.

IV. COULOMB REPULSION EFFECTS

In realistic systems the repulsive on-dot interactions $U_j\hat{n}_{j\uparrow}\hat{n}_{j\downarrow}$ would compete with the proximity-induced electron pairing, affecting the subgap bound states. Under stationary conditions this issue has been investigated by various methods (see, e.g., Ref. [31] for a survey). In particular, the considerations of the DQD horizontally embedded between either normal and superconducting leads [28] or two superconductors [15] have indeed shown a remarkable influence of the correlation effects. To our knowledge, however, the transient dynamics of the correlated quantum dots in these nanostructures has not been studied yet. In this section we briefly address such problem.

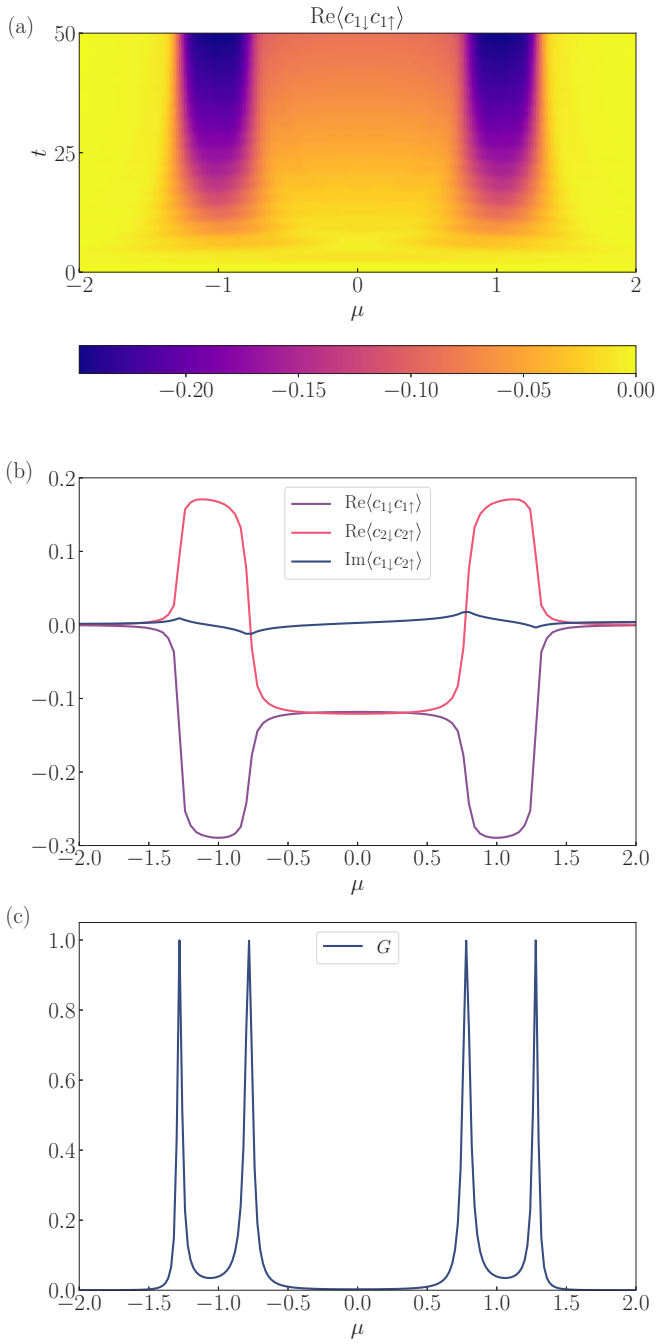

FIG. 5. (a) The real part of $\langle \hat{c}_{1\downarrow}(t)\hat{c}_{1\uparrow}(t)\rangle$ as function of the bias voltage μ and time. (b) The asymptotic ($t \to \infty$) values of $\mathrm{Re}\langle \hat{c}_{1\downarrow}(t)\hat{c}_{1\uparrow}(t)\rangle$, $\mathrm{Re}\langle \hat{c}_{2\downarrow}(t)\hat{c}_{2\uparrow}(t)\rangle$, and $\mathrm{Im}\langle \hat{c}_{1\downarrow}(t)\hat{c}_{2\uparrow}(t)\rangle$. (c) The stationary limit value of the differential conductance as a function of μ. Results are obtained for $\Gamma_N = 0.1$, $\Gamma_S = 1$, $V_{12} = 1$, $\varepsilon_{j\sigma} = 0$.

The essential features due to the quench dynamics of a correlated single quantum dot placed in the superconducting nanojunctions have been previously explored in a perturbative framework [54]. The perturbative approach, formulated in an appropriate way, could qualitatively reproduce the results of such sophisticated methods as NRG-type calculations [55]. This fact encouraged us to perform the lowest-order perturbative analysis for the same set of model parameters as used in Ref. [28], focusing on the symmetric case, $\varepsilon_{j\sigma} = -U/2$ ($U \equiv U_1 = U_2$), where the Coulomb repulsion is most efficient. For $U < 2\Gamma_S$, $\Gamma_N = \Gamma_S$, and $V_{12}/\Gamma_N = 0.5$–2, we have computed the linear conductance as a function of V_{12}, qualitatively reproducing the NRG results [28]. Obviously our mean-field study (23) is reliable only in the weak-interaction case, $U < \Gamma_\beta$. In particular, for $U < \Gamma_S$, the system is dominated by the Andreev scattering, whereas for $U > 2\Gamma_S$ the Kondo physics plays a major role [15,28].

To treat the correlation effects, we first make use of the Hartree-Fock-Bogoliubov (HFB) decoupling scheme

$$\hat{n}_{j\uparrow}\hat{n}_{j\downarrow} \simeq \hat{n}_{j\uparrow}\, n_{j\downarrow}(t) + \hat{n}_{j\downarrow}\, n_{j\uparrow}(t) + \hat{c}^\dagger_{j\uparrow}\hat{c}^\dagger_{j\downarrow}\langle \hat{c}_{j\downarrow}\hat{c}_{j\uparrow}\rangle + \hat{c}_{j\downarrow}\hat{c}_{j\uparrow}\langle \hat{c}^\dagger_{j\uparrow}\hat{c}^\dagger_{j\downarrow}\rangle, \quad (23)$$

which yields the renormalized energy levels $\tilde{\varepsilon}_{j\sigma}(t) = \varepsilon_{j\sigma} + U_j n_{j\bar{\sigma}}(t)$, where $\bar{\sigma}$ stands for the opposite spin to σ, and important corrections to the time-dependent pairing potentials $\Delta_1(t) = \Gamma_S/2 - U_1\langle \hat{c}_{1\downarrow}(t)\hat{c}_{1\uparrow}(t)\rangle$ and $\Delta_2(t) = -U_2\langle \hat{c}_{2\downarrow}(t)\hat{c}_{2\uparrow}(t)\rangle$. Combining the interactions with the superconducting proximity effect can be effectively described by the following Hamiltonian,

$$\hat{H}^{\mathrm{HFB}} \approx \sum_{j,\sigma} \tilde{\varepsilon}_{j\sigma}(t)\hat{c}^\dagger_{j\sigma}\hat{c}_{j\sigma} - \sum_j \left(\Delta_j(t)\hat{c}^\dagger_{j\uparrow}\hat{c}^\dagger_{j\downarrow} + \mathrm{H.c.}\right) + \sum_\sigma \left[\left(V_{12}\hat{c}^\dagger_{1\sigma} + \sum_{\mathbf{k}} V_{N\mathbf{k}}\hat{c}^\dagger_{N\mathbf{k}\sigma}\right)\hat{c}_{2\sigma} + \mathrm{H.c.}\right] + \hat{H}_N, \quad (24)$$

where the time-dependent energy levels $\tilde{\varepsilon}_{j\sigma}(t)$ and on-dot pairings $\Delta_j(t)$ must be determined numerically. We have self-consistently computed the time-dependent $n_{j\sigma}(t)$, $\langle \hat{c}_{j\downarrow}(t)\hat{c}_{j\uparrow}(t)\rangle$, the current $j_{N\sigma}(t)$, and its differential conductance $G_\sigma(\mu, t)$, using the procedure outlined by us in Ref. [51] (see Appendix B). For this purpose we have solved the differential equations of motion for $n_{j\sigma}(t)$, $\langle \hat{c}_{j\downarrow}(t)\hat{c}_{j\uparrow}(t)\rangle$, and $\langle \hat{c}^\dagger_{1\sigma}(t)\hat{c}_{2\sigma}(t)\rangle$ at intermediate steps computing also the correlation functions $\langle \hat{c}^\dagger_{1\sigma}(t)\hat{c}_{N\mathbf{k}\sigma}(0)\rangle$, $\langle \hat{c}_{1\sigma}(t)\hat{c}_{N\mathbf{k}\bar{\sigma}}(0)\rangle$, $\langle \hat{c}^\dagger_{2\sigma}(t)\hat{c}_{N\mathbf{k}\sigma}(0)\rangle$, and $\langle \hat{c}_{2\sigma}(t)\hat{c}_{N\mathbf{k}\bar{\sigma}}(0)\rangle$. We have calculated these quantities iteratively within the Runge-Kutta algorithm, starting from their initial ($t = 0$) values.

Figure 6 displays the typical evolution of the differential conductance obtained for several values of the Coulomb potential, assuming small, $V_{12} = 0.5$, and large, $V_{12} = 2$, interdot couplings. As the Andreev conductance is symmetric with respect to the bias voltage, $G(\mu, t) = G(-\mu, t)$, we show its variation only for the positive bias μ where all dynamical features can be well recognized. Upon increasing the Coulomb repulsion U ($U_1 = U_2 \equiv U$), the two-peak structure (characteristic for the noninteracting system) undergoes a gradual reconstruction into a single broad peak. This tendency indicates that the Coulomb repulsion suppresses the effects caused by both the interdot hybridization and the superconducting proximity effect. The time needed for the development of such final structure (observable in the differential conductance with respect to the bias voltage μ) turns out to be $\sim 100\hbar/\Gamma_S$. For the experimentally realistic coupling $\Gamma_S \sim 200$ μeV, this characteristic timescale would be 0.3–0.4 μsec.

For more credible determination of the correlation effects beyond the perturbative framework, we have additionally

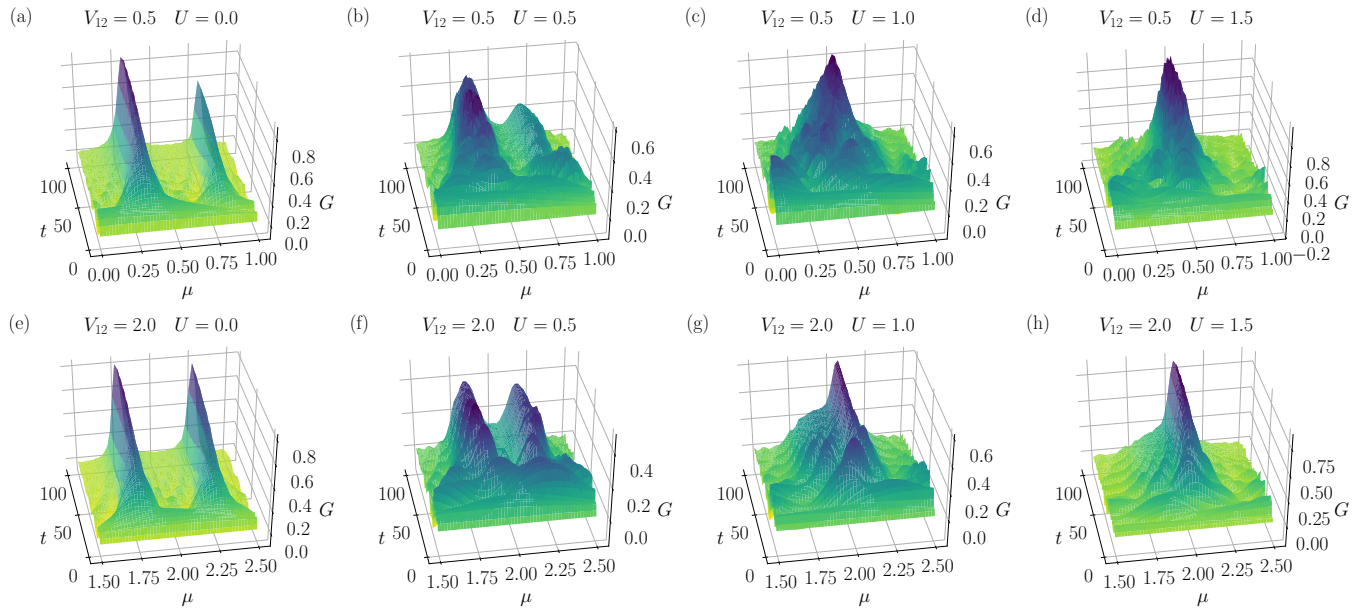

FIG. 6. The time-dependent differential conductance $G(\mu, t)$ (in units of $2e^2/h$) as a function the bias voltage μ obtained in the weak $V_{12} = 0.5$ (upper panels) and strong interdot coupling limit $V_{12} = 2$ (bottom panels) for several values of the Coulomb potential (as indicated), assuming $\varepsilon_{j\sigma} = -U/2$, $\Gamma_N = 0.1$, and $\Gamma_S \equiv 1$.

used the time-dependent numerical renormalization group technique [48–50,56–59]. This approach allows for treating correlations in a very accurate manner; however, it is restricted to unbiased junctions. The tNRG employs the Wilson's numerical renormalization group (NRG) method to solve the initial ($\hat{H}_0$) and final ($\hat{H}$) Hamiltonians essential to evaluate the quench dynamics according to the general form of time-dependent Hamiltonian

$$\hat{H}(t) = \theta(-t)\hat{H}_0 + \theta(t)\hat{H}. \tag{25}$$

The diagonalization of both Hamiltonians is performed in N iterations with N_K energetically lowest-lying eigenstates retained at each iteration. These kept eigenstates, tagged with superscript K, are used in consecutive iterations to build new product states corresponding to the addition of another site of the Wilson chain. The remaining states are referred to as discarded, as well as all states from the last iteration of the procedure, and are tagged with superscript D. All discarded states of the corresponding Hamiltonians are used to span the full many-body initial and final eigenbases [49],

$$\sum_{nse} |nse\rangle_0^D {}_0^D\langle nse| = \hat{\mathbb{1}} \quad \text{and} \quad \sum_{nse} |nse\rangle^D {}^D\langle nse| = \hat{\mathbb{1}}. \tag{26}$$

Here, the index s refers to the eigenstates obtained at the nth iteration and the index e expresses the environmental part of the Wilson chain. Due to the energy-scale separation, these eigenstates are good approximations of the eigenstates of the full NRG Hamiltonians.

We have computed the dynamical quantities of the unbiased N-DQD-S heterostructure, determining the expectation values of the observables in frequency domain $O(\omega) \equiv \langle\hat{\mathcal{O}}(\omega)\rangle$. The formula for $O(\omega)$ in terms of the designated eigenstates can be written as

$$O(\omega) = \sum_{n}^{XX' \neq KK} \sum_{n'} \sum_{ss'e} {}^X\langle nse|w_{n'}\hat{\rho}_{0n'}|ns'e\rangle^{X'} \times {}^{X'}\langle ns'e|\hat{\mathcal{O}}|nse\rangle^X \, \delta\left(\omega + E_{ns}^X - E_{ns'}^{X'}\right). \tag{27}$$

Here, $\hat{\rho}_{0n'}$ denotes the contribution to the initial density matrix from the n'th iteration and $w_{n'}$ is the corresponding weight after tracing out the environmental states, while the initial full density matrix $\hat{\rho}_0$ built from $\hat{H}_0$ at thermal equilibrium reads [60]

$$\hat{\rho}_0 = \sum_{nse} \frac{e^{-\beta E_{0ns}^D}}{Z} |nse\rangle_0^D {}_0^D\langle nse|, \tag{28}$$

where $\beta \equiv (k_B T)^{-1}$ is the inverse temperature and $Z \equiv \sum_{nse} e^{-\beta E_{0ns}^D}$ is the partition function.

In the following steps, the obtained collection of Dirac delta peaks with corresponding weights is weakly smoothed with a log-Gaussian function and broadening parameter $b \leqslant 0.1$. Finally, a Fourier transformation back into the time domain is applied [61],

$$O(t) = \int_{-\infty}^{\infty} O(\omega) e^{-i\omega t} d\omega. \tag{29}$$

In performed tNRG calculations we have assumed the discretization parameter $\Lambda = 2$, the length of the Wilson chain to consist of $N = 100$ sites, and we have kept $N_K = 2000$ eigenstates at each iteration. More detailed description of the tNRG implementation and technicalities has been discussed in Ref. [62].

Figure 7 presents the real/imaginary parts of the electron pairing induced on individual quantum dots (the upper and middle panels) and between them (the bottom panels) for

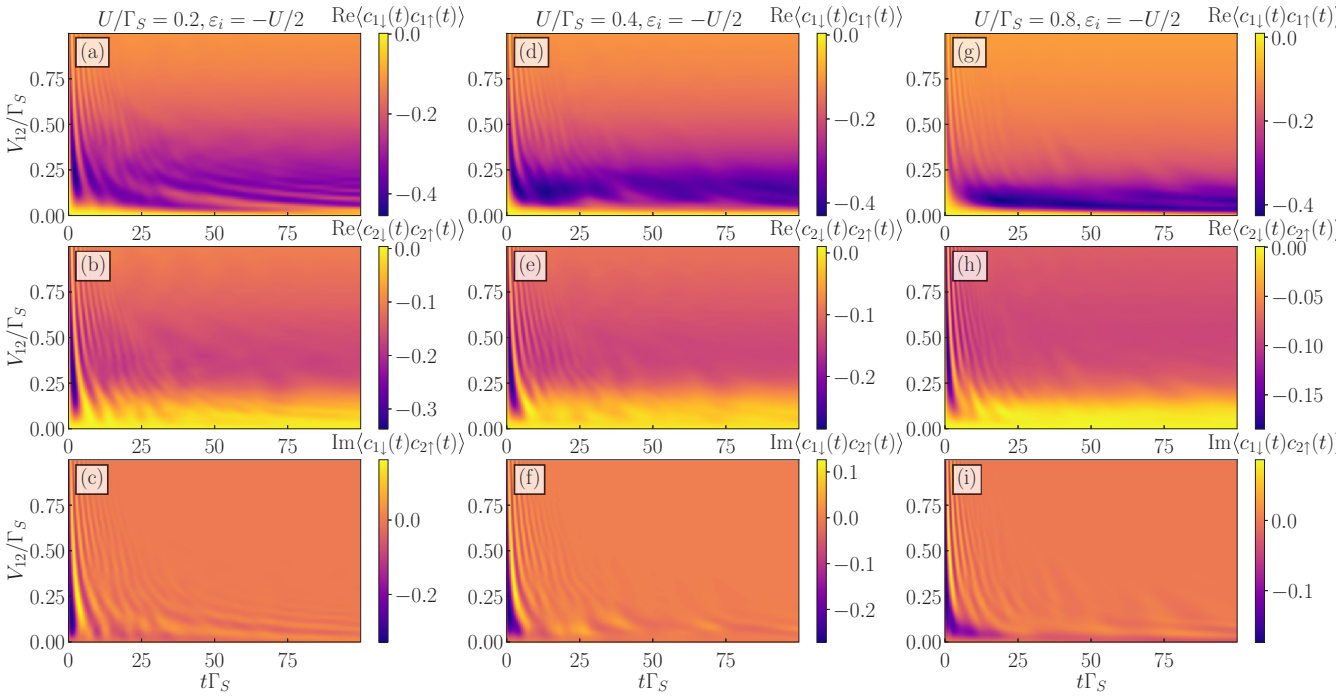

FIG. 7. The real part of the on-dot pairings $\langle \hat{c}_{j\downarrow}(t)\hat{c}_{j\uparrow}(t)\rangle$ (top and middle panels) and imaginary part of the interdot pairing $\langle \hat{c}_{1\downarrow}(t)\hat{c}_{2\uparrow}(t)\rangle$ (bottom panel) with respect to time (horizontal axis) and the coupling V_{12} (vertical axis). Results are obtained by tNRG calculations for several values of the Coulomb potential (as indicated), assuming the half-filled quantum dots $\varepsilon_j = -U/2$ and $\Gamma_N/\Gamma_S = 0.1$.

three different values of Coulomb potential: $U/\Gamma_S = 0.2, 0.4$, and 0.8. Here, we annotate that for tNRG results we have evaluated the quench exclusively in the coupling to the superconducting lead Γ_S. Other couplings are assumed to be time-independent and have values as specified in Fig. 7. This modification of the quench protocol allowed us to remove weak and nonrelevant dynamics associated with switching on other couplings, while the role of the superconducting correlations is now more evident. We checked numerically that in both scenarios the results and conclusions are in agreement.

We clearly notice that repulsive interactions suppress the pairings of all these channels. Comparison of these quantities against time at some fixed interdot coupling (for instance $V_{12} = 0.5$) indicates that the quantum oscillations become faster upon increasing the Coulomb potential U. This speedup of quantum oscillations stems from renormalization of the in-gap state energies observable also in the mean-field calculations (Fig. 6). Additionally, we notice that the region of transient effects gradually shrinks with increasing the Coulomb potential. The latter effect can be indirectly assigned to suppression of the superconducting proximity effect (recall that the quantum oscillations are here driven by Rabi-type transitions between pairs of in-gap bound states).

The interdot coupling V_{12} plays an important role in the distribution of the on-dot pairing potential between the coupled quantum dots. For relatively weak values, $V_{12}/\Gamma_S < 0.25$, the strong on-dot pairing potential is present on the quantum dot directly coupled to the superconductor, while the second dot is almost unaffected by the proximity effect. However, as the interdot coupling is amplified, it mediates the superconducting correlations onto the second dot. For values $V_{12}/\Gamma_S > 0.5$, the on-dot pairing potential is more evenly distributed between both dots. This observation reveals the crucial role of interdot coupling in transferring the superconducting correlations. Another very important feature can be seen for the weak interdot coupling. For all pairing channels we clearly notice blockade of the superconducting proximity effect, strictly due to the initial single occupancy of both quantum dots. This brings us to the important conclusion that dynamical signatures of the triplet/Andreev blockade should be well observable in the correlated N-DQD-S nanostructures, whenever the coupling between the quantum dots is weak.

Summarizing this section, we emphasize that a competition of the repulsive on-dot interactions with the superconducting proximity effect is evident, both in the stationary and dynamical properties. The magnitude of electron pairing induced on each quantum dot and between them is considerably suppressed by the interactions. Furthermore, the quantum oscillations become faster and transient phenomena survive over some narrower time region upon increasing the Coulomb potential.

V. SUMMARY AND OUTLOOK

We have investigated the dynamical effects observable in the double quantum dot (DQD) abruptly embedded between the superconducting and metallic leads. Transient phenomena of the uncorrelated setup have been explored by solving the coupled equations of motion, treating the initial constraints within the Laplace transform approach. Focusing on the subgap regime, we have derived analytical expressions for the charge occupancy of both quantum dots, the induced on-dot and interdot electron pairings, and the currents flowing between neighboring constituents of N-DQD-S heterostructure.

The time-dependent quantities (except the differential conductance) have been represented by contributions, dependent on the initial DQD fillings and on their couplings to the external leads. These expressions guided us to identify the characteristic timescales of transient phenomena, manifested by (i) the Rabi-type quantum oscillations due to transitions between the pairs of in-gap bound states and (ii) the relaxation processes involving a continuous spectrum of the metallic lead.

To single out the quantum oscillations, we have analyzed them for a DQD coupled only to the superconducting reservoir (Appendix C). Under such circumstances all physical quantities would be periodic in time, unless the higher-energy electronic states from outside the pairing gap were taken into consideration [54]. Our analytical expressions (C28)–(C30) indicate that the on-dot pairing functions are purely imaginary whereas the interdot pairing function is purely real. We have investigated the components of quantum oscillations in the strong $V_{12} > \Gamma_S$ and weak $V_{12} < \Gamma_S$ interdot couplings, respectively. Furthermore, we have also inspected under what circumstances the superconducting proximity effect is going to be blocked, preventing the Cooper pairs from leaking onto the quantum dots. We have found that for the initial triplet configuration of the DQD-S system, the charge flow $j_{S\sigma}(t)$ between the superconducting lead and neighboring quantum dot is completely forbidden.

In the N-DQD-S junctions a similar blockade is still present, although in a less severe version because electrons can flow back and forth to/from the normal lead. Under the stationary conditions such *triplet blockade* has been reported experimentally in the Josephson (S-DQD-S) junction [16] and its analog, the so called *Andreev blockade*, has been recently evidenced for N-DQD-S heterostructure [17]. Suppression of the superconducting proximity effect occurs also in the presence of the correlations, especially in the weak interdot coupling regime. Additionally, we have shown that the time-resolved Andreev conductance can probe a buildup of the in-gap bound states and indirectly detect the dynamical superconducting proximity effect.

In future it would be worthwhile to study transient phenomena of the interacting quantum dots, focusing on the parity crossings and realization of the subgap Kondo effect. We hope that our analytical results obtained for the noninteracting system could serve as a useful benchmark for such project. Another challenging issue can be related to the Majorana-type versions of the in-gap bound states [63] with appealing perspectives to use them in semiconductor-based superconducting qubits and quantum computing [64].

ACKNOWLEDGMENTS

This work was supported by the National Science Centre (NCN, Poland) under Grants No. UMO-2017/27/B/ST3/01911 (R.T., B.B.), No. UMO-2018/29/N/ST3/01038 (K.W.), and No. UMO-2018/29/B/ST3/00937 (I.W., T.D.).

APPENDIX A: LAPLACE TRANSFORMS

We derive here the Laplace transforms for $\hat{c}_{j\sigma}(s)$ and $\hat{c}_{S\mathbf{q}/N\mathbf{k}\sigma}(s)$ required for the determination of the time-dependent physical quantities discussed in this paper. Upon transforming the Heisenberg equations we obtain

$$(s+i\varepsilon_{1\uparrow})\hat{c}_{1\uparrow}(s) = -i\sum_{\mathbf{q}} V_{S\mathbf{q}}\hat{c}_{S\mathbf{q}\uparrow}(s) - iV_{12}\hat{c}_{2\uparrow}(s) + \hat{c}_{1\uparrow}(0), \tag{A1}$$

$$(s-i\varepsilon_{1\downarrow})\hat{c}^{\dagger}_{1\downarrow}(s) = i\sum_{\mathbf{q}} V_{S\mathbf{q}}\hat{c}^{\dagger}_{S\mathbf{q}\downarrow}(s) + iV_{12}\hat{c}^{\dagger}_{2\downarrow}(s) + \hat{c}^{\dagger}_{1\downarrow}(0), \tag{A2}$$

$$(s+i\varepsilon_{S\mathbf{q}})\hat{c}_{S\mathbf{q}\uparrow}(s) = -iV_{S\mathbf{q}}\hat{c}_{1\uparrow}(s) - i\Delta\hat{c}^{\dagger}_{S-\mathbf{q}\downarrow}(s) + \hat{c}_{S\mathbf{q}\uparrow}(0), \tag{A3}$$

$$(s-i\varepsilon_{S\mathbf{q}})\hat{c}^{\dagger}_{S-\mathbf{q}\downarrow}(s) = iV_{S\mathbf{q}}\hat{c}^{\dagger}_{1\downarrow}(s) - i\Delta\hat{c}_{S\mathbf{q}\uparrow}(s) + c^{\dagger}_{S-\mathbf{q}\downarrow}(0), \tag{A4}$$

and

$$(s+i\varepsilon_{2\uparrow})\hat{c}_{2\uparrow}(s) = -i\sum_{\mathbf{k}} V_{N\mathbf{k}}\hat{c}_{N\mathbf{k}\uparrow}(s) - iV_{12}\hat{c}_{1\uparrow}(s) + \hat{c}_{2\uparrow}(0), \tag{A5}$$

$$(s-i\varepsilon_{2\downarrow})\hat{c}^{\dagger}_{2\downarrow}(s) = i\sum_{\mathbf{k}} V_{N\mathbf{k}}\hat{c}^{\dagger}_{N\mathbf{k}\downarrow}(s) + iV_{12}\hat{c}^{\dagger}_{1\downarrow}(s) + \hat{c}^{\dagger}_{2\downarrow}(0), \tag{A6}$$

$$(s+i\varepsilon_{N\mathbf{k}})\hat{c}_{N\mathbf{k}\uparrow}(s) = -iV_{N\mathbf{k}}\hat{c}_{2\uparrow}(s) + \hat{c}_{N\mathbf{k}\uparrow}(0), \tag{A7}$$

$$(s-i\varepsilon_{N\mathbf{k}})\hat{c}^{\dagger}_{N\mathbf{k}\downarrow}(s) = iV_{N\mathbf{k}}\hat{c}^{\dagger}_{2\downarrow}(s) + \hat{c}^{\dagger}_{N\mathbf{k}\downarrow}(0). \tag{A8}$$

Equations (A1)–(A4) are coupled to (A5)–(A8) through the interdot coupling V_{12}. After some lengthy but straightforward algebra, we can simplify them to the following compact form:

$$\left(s+i\varepsilon_{S\mathbf{q}\uparrow} + \sum_{\mathbf{q}} \frac{V^2_{S\mathbf{q}}(s-i\varepsilon_{S\mathbf{q}})}{s^2+\varepsilon^2_{S\mathbf{q}}+\Delta^2}\right)\hat{c}_{1\uparrow}(s)$$
$$= -\sum_{\mathbf{q}} \frac{V^2_{S\mathbf{q}}\Delta}{s^2+\varepsilon^2_{S\mathbf{q}}+\Delta^2}\hat{c}^{\dagger}_{1\downarrow}(s) - iV_{12}\hat{c}_{2\uparrow}(s) + \hat{a}_1, \tag{A9}$$

$$\left(s-i\varepsilon_{1\downarrow} + \sum_{\mathbf{q}} \frac{V^2_{S\mathbf{q}}(s+i\varepsilon_{S\mathbf{q}})}{s^2+\varepsilon^2_{S\mathbf{q}}+\Delta^2}\right)\hat{c}^{\dagger}_{1\downarrow}(s)$$
$$= -i\sum_{\mathbf{q}} \frac{V^2_{S\mathbf{q}}\Delta}{s^2+\varepsilon^2_{S\mathbf{q}}+\Delta^2}\hat{c}_{1\uparrow}(s) + iV_{12}\hat{c}^{\dagger}_{2\downarrow}(0) + \hat{a}_2, \tag{A10}$$

$$\left(s+i\varepsilon_{2\uparrow} + \sum_{\mathbf{k}} \frac{V^2_{N\mathbf{k}}}{s+i\varepsilon_{N\mathbf{k}}}\right)\hat{c}_{2\uparrow}(s) = -iV_{12}\hat{c}_{1\uparrow}(s) + \hat{a}_3, \tag{A11}$$

$$\left(s-i\varepsilon_{2\uparrow} + \sum_{\mathbf{k}} \frac{V^2_{N\mathbf{k}}}{s-i\varepsilon_{N\mathbf{k}}}\right)\hat{c}^{\dagger}_{2\downarrow}(s) = iV_{12}\hat{c}_{1\downarrow}(s) + \hat{a}_4, \tag{A12}$$

where the last components are defined as

$$\hat{a}_1 = \hat{c}_{1\uparrow}(0) - \sum_{\mathbf{q}} \frac{V_{S\mathbf{q}}\Delta}{s^2+\varepsilon_{S\mathbf{q}}^2+\Delta^2}\hat{c}^\dagger_{S-\mathbf{q}\downarrow}(0) - i\sum_{\mathbf{q}} \frac{V_{S\mathbf{q}}(s-i\varepsilon_{S\mathbf{q}})}{s^2+\varepsilon_{S\mathbf{q}}^2+\Delta^2}\hat{c}_{S\mathbf{q}\uparrow}(0), \tag{A13}$$

$$\hat{a}_2 = \hat{c}^\dagger_{1\downarrow}(0) + \sum_{\mathbf{q}} \frac{V_{S\mathbf{q}}\Delta}{s^2+\varepsilon_{S\mathbf{q}}^2+\Delta^2}\hat{c}_{S-\mathbf{q}\uparrow}(0) + i\sum_{\mathbf{q}} \frac{V_{S\mathbf{q}}(s+i\varepsilon_{S\mathbf{q}})}{s^2+\varepsilon_{S\mathbf{q}}^2+\Delta^2}\hat{c}^\dagger_{S\mathbf{q}\downarrow}(0), \tag{A14}$$

$$\hat{a}_3 = -i\sum_{\mathbf{k}} \frac{V_{N\mathbf{k}}}{s+i\varepsilon_{N\mathbf{k}}}\hat{c}_{N\mathbf{k}\uparrow}(0) + \hat{c}_{2\uparrow}(0), \tag{A15}$$

$$\hat{a}_4 = i\sum_{\mathbf{k}} \frac{V_{N\mathbf{k}}}{s-i\varepsilon_{N\mathbf{k}}}\hat{c}^\dagger_{N\mathbf{k}\downarrow}(0) + \hat{c}^\dagger_{2\downarrow}(0). \tag{A16}$$

In the wide-bandwidth limit we can perform summations over momenta $\mathbf{k}$ and $\mathbf{q}$ of the itinerant electrons. In this way we obtain the set of coupled equations (6)–(9) presented in the main part of this paper.

APPENDIX B: INTERDOT CHARGE FLOW AND SUPERCURRENT

Here we provide detailed expressions for the interdot current $j_{12\sigma}(t)$ and the current $j_{S\sigma}(t)$ between QD_1 and superconductor. The charge flow $j_{12\sigma}(t)$ between the quantum dots can be calculated from

$$j_{12\sigma}(t) = -2V_{12}\mathrm{Im}\langle\hat{c}^\dagger_{1\sigma}(t)\hat{c}_{2\sigma}(t)\rangle. \tag{B1}$$

Using the inverse Laplace transforms of $\hat{c}_{j\sigma}(s)$ operators [Eqs. (10) and (11)] we obtain

$$\begin{aligned} j_{12\uparrow/\downarrow}(t) = -2V_{12}^2\mathrm{Re}\Bigg[& n_{1\uparrow/\downarrow}(0)\mathcal{L}^{-1}\left\{\frac{u(s)(s+\Gamma_N/2)}{W(s)}\right\}(t)\cdot\mathcal{L}^{-1}\left\{\frac{u(s)}{W(s)}\right\}(t) - n_{2\uparrow/\downarrow}(0)\mathcal{L}^{-1}\left\{\frac{u(s)}{W(s)}\right\}(t) \\ & \times\mathcal{L}^{-1}\left\{\frac{1}{s+\Gamma_N/2}\left(1-\frac{u(s)V_{12}^2}{W(s)}\right)\right\}(t) + [1-n_{1\downarrow/\uparrow}(0)]\Gamma_S^2/4\mathcal{L}^{-1}\left\{\frac{(s+\Gamma_N/2)^2}{W(s)}\right\}(t)\cdot\mathcal{L}^{-1}\left\{\frac{s+\Gamma_N/2}{W(s)}\right\}(t) \\ & + V_{12}^2\Gamma_S^2/4[1-n_{2\downarrow/\uparrow}(0)]\mathcal{L}^{-1}\left\{\frac{s+\Gamma_N/2}{W(s)}\right\}(t)\cdot\mathcal{L}^{-1}\left\{\frac{1}{W(s)}\right\}(t) \\ & + \Gamma_N\Gamma_S^2V_{12}^2/8\pi\int_{-\infty}^{\infty}d\varepsilon[1-f_N(\varepsilon)]\mathcal{L}^{-1}\left\{\frac{s+\Gamma_N/2}{(s+i\varepsilon)W(s)}\right\}(t)\cdot\mathcal{L}^{-1}\left\{\frac{1}{(s-i\varepsilon)W(s)}\right\}(t) \\ & + \frac{\Gamma_N}{\pi}\int_{-\infty}^{\infty}d\varepsilon f_N(\varepsilon)\mathcal{L}^{-1}\left\{\frac{u(s)}{W(s)(s-i\varepsilon)}\right\}(t)\cdot\mathcal{L}^{-1}\left\{\left(\frac{V_{12}^2u(s)}{W(s)}-1\right)\left(\frac{1}{(s+i\varepsilon)(s+\Gamma_N/2)}\right)\right\}(t)\Bigg]. \end{aligned} \tag{B2}$$

In a similar way, the current flowing from the superconducting lead to the first quantum dot is given by

$$j_{S\sigma}(t) = 2\mathrm{Im}\left[\sum_{\mathbf{q}} V_{S\mathbf{q}}\langle\hat{c}^\dagger_{1\sigma}(t)\hat{c}_{S\mathbf{q}\sigma}(t)\rangle\right], \tag{B3}$$

where $\hat{c}^\dagger_{1\sigma}(t)$ should be taken from the inverse Laplace transform of the Hermitian conjugation of (10). The inverse Laplace transform of $\hat{c}_{S\mathbf{q}\sigma}(s)$, calculated from Eqs. (A1)–(A8), takes the following form:

$$\hat{c}_{S\mathbf{q}\uparrow}(s) = \frac{1}{s^2+\varepsilon_{S\mathbf{q}}^2+\Delta^2}\left[-iV_{S\mathbf{q}}(s-i\varepsilon_{S\mathbf{q}})\hat{c}_{1\uparrow} + V_{S\mathbf{q}}\Delta\hat{c}^\dagger_{1\downarrow}(s) - i\Delta\hat{c}^\dagger_{S-\mathbf{q}\downarrow}(0) + (s-i\varepsilon_{S\mathbf{q}})\hat{c}_{S\mathbf{q}\uparrow}(0)\right]. \tag{B4}$$

In the limit $\Delta\to\infty$ we obtain

$$\begin{aligned} j_{S\sigma}(t) = \frac{\Gamma_S^2}{2}\mathrm{Re}\Bigg[& [1-n_{1\sigma}(0)-n_{1-\sigma}(0)]\mathcal{L}^{-1}\left\{\frac{(s+\Gamma_N/2)^2}{W(s)}\right\}(t)\cdot\mathcal{L}^{-1}\left\{\frac{(s+\Gamma_N/2)u(s)}{W(s)}\right\}(t) \\ & + V_{12}^2[1-n_{2\sigma}(0)-n_{2-\sigma}(0)]\mathcal{L}^{-1}\left\{\frac{s+\Gamma_N/2}{W(s)}\right\}(t)\cdot\mathcal{L}^{-1}\left\{\frac{u(s)}{W(s)}\right\}(t) \\ & + \frac{\Gamma_NV_{12}^2}{2\pi}\int_{-\infty}^{\infty}d\varepsilon[1-2f_N(\varepsilon)]\mathcal{L}^{-1}\left\{\frac{s+\Gamma_N/2}{(s+i\varepsilon)W(s)}\right\}(t)\cdot\mathcal{L}^{-1}\left\{\frac{u(s)}{(s-i\varepsilon)W(s)}\right\}(t)\Bigg]. \end{aligned} \tag{B5}$$

Since the supercurrent $j_{S\sigma}(t)$ originates from tunneling of electron pairs, therefore $j_{S\uparrow}(t) = j_{S\downarrow}(t)$.

APPENDIX C: DQD COUPLED TO SUPERCONDUCTOR

Let us consider the case of $\Gamma_N = 0$. Under such circumstances, one can derive the analytical expressions for observables, which well illustrate the dynamics induced by an abrupt coupling to the superconducting lead.

For $\Gamma_N = 0$, Eqs. (12) and (13) simplify to

$$u(s) = s^2 + V_{12}^2, \tag{C1}$$

$$W(s) = \left(s^2 + V_{12}^2\right)^2 + \Gamma_S^2 s^2/4. \tag{C2}$$

The complex roots of (11) are given by $s_{1,2} = \pm i\bar{s}_1$ and $s_{3,4} = \pm i\bar{s}_3$, where

$$\bar{s}_{1,3} = \frac{1}{2}\left(\sqrt{4V_{12}^2 + \Gamma_S^2/4} \mp \frac{\Gamma_S}{2}\right); \tag{C3}$$

thus the inverse Laplace transforms $\mathcal{L}^{-1}\{\hat{c}_{j\sigma}^{(\dagger)}(s)\}(t)$ can be obtained explicitly. In what follows, we analyze the expectation values of various quantities, showing that they periodically oscillate in time with the characteristic frequencies. In the absence of a metallic lead ($\Gamma_N = 0$), the last two terms of Eqs. (14) and (15) vanish; therefore $n_{j\sigma}(t)$ simplifies to

$$\begin{aligned} n_{1\uparrow/\downarrow}(t) = \frac{1}{g_s^2\left(4V_{12}^2 + g_s^2\right)}\big\{ & n_{1\uparrow/\downarrow}(0)[\alpha_1\cos(\bar{s}_1 t) - \alpha_3\cos(s_3 t)]^2 + n_{2\uparrow/\downarrow}(0)V_{12}^2 g_s^2[\sin(\bar{s}_1 t) + \sin(\bar{s}_3 t)]^2 \\ & + [1 - n_{1\downarrow/\uparrow}(0)]g_s^2[\bar{s}_1\sin(\bar{s}_1 t) - \bar{s}_3\sin(s_3 t)]^2 + [1 - n_{2\downarrow/\uparrow}(0)]g_s^2 V_{12}^2[\cos(\bar{s}_1 t) - \cos(\bar{s}_3 t)]^2\big\}, \end{aligned} \tag{C4}$$

$$\begin{aligned} n_{2\uparrow/\downarrow}(t) = \frac{1}{\left(4V_{12}^2 + g_s^2\right)}\big\{ & n_{1\uparrow/\downarrow}(0)V_{12}^2[\sin(\bar{s}_1 t) + \sin(\bar{s}_3 t)]^2 + n_{2\uparrow/\downarrow}(0)[\bar{s}_3\cos(\bar{s}_1 t) + \bar{s}_1\cos(\bar{s}_3 t)]^2 \\ & + [1 - n_{1\downarrow/\uparrow}(0)]V_{12}^2[\cos(\bar{s}_1 t) - \cos(\bar{s}_3 t)]^2 + [1 - n_{2\downarrow/\uparrow}(0)][\bar{s}_1\sin(\bar{s}_3 t) - \bar{s}_3\sin(\bar{s}_1 t)]^2\big\}, \end{aligned} \tag{C5}$$

where $g_s = \frac{\Gamma_S}{2}$ and $\alpha_{1/3} = \frac{g_s^2}{2} \mp \frac{g_s}{2}\sqrt{g_s^2 + 4V_{12}^2}$. These expressions explicitly show an important role of the initial fillings. One can notice that for some cases, e.g., when both quantum dots are initially singly occupied by the same spin, their occupancy is completely frozen, $n_{j\sigma}(t) = n_{j\sigma}(0)$. This is physically obvious, because the electron occupying QD_1 is neither allowed to hop to QD_2 nor to the superconducting lead.

We now consider two different initial configurations, namely (i) $n_{j\sigma}(0) = 0$ or $n_{j\sigma}(0) = 1$, and (ii) $n_{1\uparrow} = 1$, $n_{1\downarrow} = 0 = n_{2\sigma}$. Note that in the first case the electron transfer between QD_1 and superconducting lead is allowed right from the very beginning. Contrary to such scenario, in the second case any transfer of electron between the superconducting lead and QD_1 would be allowed only after the spin-↑ electron jumps from QD_1 to QD_2. These initial conditions are effectively responsible for qualitatively different evolutions of $n_{j\sigma}(t)$.

For the initially empty dots Eqs. (C4) and (C5) imply

$$\begin{aligned} n_{1/2\sigma}(t) = \frac{1}{4V_{12}^2 + g_s^2}\big\{ & 4V_{12}^2\sin^2[(\bar{s}_1 - \bar{s}_3)t/2] \\ & + \alpha_{1/3}\sin^2(\bar{s}_1 t) + \alpha_{3/1}\sin^2(\bar{s}_3 t)\}, \end{aligned} \tag{C6}$$

whereas for $n_{j\sigma}(0) = 1$ we obtain

$$\begin{aligned} n_{1/2\sigma}(t) = \frac{1}{4V_{12}^2 + g_s^2}\big\{ & 4V_{12}^2\cos^2[(\bar{s}_1 - \bar{s}_3)t/2] \\ & + \alpha_{1/3}\cos^2(\bar{s}_1 t) + \alpha_{3/1}\cos^2(\bar{s}_3 t)\big\}. \end{aligned} \tag{C7}$$

We recognize here a superposition of three oscillations characterized by the periods $2\pi/|\bar{s}_1 - \bar{s}_3|$, $\pi/|\bar{s}_1|$, and $\pi/|\bar{s}_3|$ with different amplitudes. In order to clarify such time dependence let us analyze the extreme cases when V_{12} is much greater or smaller than Γ_S, respectively.

Expanding the contribution appearing in Eqs. (C6) and (C7) in powers of $x \equiv \frac{\Gamma_S}{V_{12}} \ll 1$ up to the first nonvanishing terms, one obtains, for the initially empty QDs,

$$n_{1/2\sigma}(t) \simeq \sin^2\left(\frac{\Gamma_S}{4}t\right) \pm \frac{x}{8}\sin\left(\frac{\Gamma_S}{2}t\right)\sin\left(\sqrt{4V_{12}^2 + g_s^2}t\right), \tag{C8}$$

and, for the initially singly occupied dots $n_{j\sigma}(0) = 1$,

$$n_{1/2\sigma}(t) \simeq \cos^2\left(\frac{\Gamma_S}{4}t\right) \mp \frac{x}{8}\sin\left(\frac{\Gamma_S}{2}t\right)\sin\left(\sqrt{4V_{12}^2 + g_s^2}t\right). \tag{C9}$$

We notice that $n_{j\sigma}(t)$ are governed mainly by the functions $\sin^2(\frac{\Gamma_S}{4}t)$ or $\cos^2(\frac{\Gamma_S}{4}t)$ with the period $T = 4\pi/\Gamma_S$. One may argue, however, that for $V_{12} \gg \Gamma_S$ these occupancies should oscillate vs time in a way typical for a two-level system, characterized by the period $T = \pi/V_{12}$. In fact such component is present here in the form of small correction, proportional to $\pm\frac{1}{8}\frac{\Gamma_S}{V_{12}}\sin(\frac{\Gamma_S}{2}t)$ with the period $\sim\frac{\pi}{V_{12}}$. Some difference between the results obtained for the isolated two-level system in comparison to the present case manifests itself through influence of the initial occupancies of QDs.

A similar analysis for the opposite limit, $\frac{1}{x} \ll 1$, yields

$$\begin{aligned} n_{1/2\sigma}(t) \simeq \sin^2(\bar{s}_{3/1}t) + x^{-2}\Bigg[& 16\sin^2\left(\frac{\Gamma_S}{4}t\right) \\ & - 4\sin^2(\bar{s}_{1/3}t) - 12\sin^2(\bar{s}_{3/1}t)\Bigg], \end{aligned} \tag{C10}$$

for the initially empty dots, and

$$\begin{aligned} n_{1/2\sigma}(t) \simeq \cos^2(\bar{s}_{3/1}t) + x^{-2}\Bigg[& 16\cos^2\left(\frac{\Gamma_S}{4}t\right) \\ & - 4\cos^2(\bar{s}_{1/3}t) - 12\cos^2(\bar{s}_{3/1}t)\Bigg], \end{aligned} \tag{C11}$$

for the initially filled dots. Time-dependent occupancy of QD_1 reveals the dominant quantum oscillations with period $T = 2\pi/(\sqrt{4V_{12}^2 + g_s^2} + g_s)$. This result can be compared with the

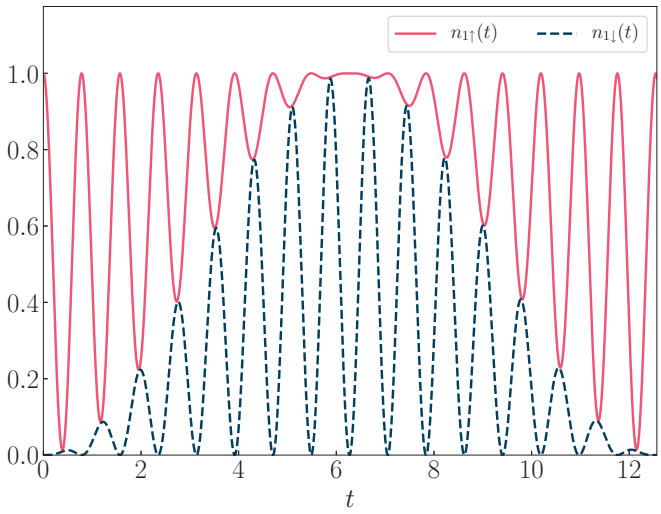

FIG. 8. Time-dependent occupancies $n_{1\uparrow}(t)/n_{1\downarrow}(t)$ (shown by the solid/dashed lines) induced by the sudden switching of Γ_S and interdot coupling V_{12}. Results are obtained for $\varepsilon_{j\sigma} = 0$, $\Gamma_N = 0$, $\Gamma_S = 1$, $V_{12} = 4$ assuming the initial configuration $n_{1\uparrow}(0) = 1$ and $n_{1\downarrow}(0) = 0 = n_{2\sigma}(0)$.

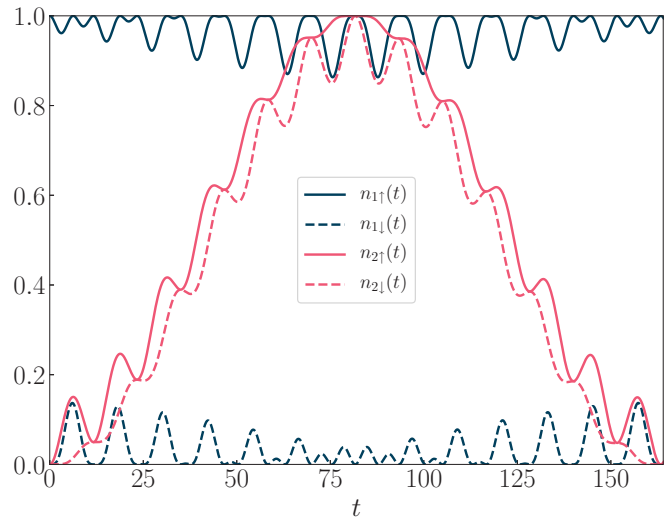

FIG. 9. Time-dependent occupancies $n_{j\sigma}(t)$ (see the legend) obtained for the weak interdot coupling $V_{12} = 0.1\Gamma_S$ using the same set of model parameters as in Fig. 8.

oscillations of a single quantum dot proximitized to the superconducting lead, whose period is $2\pi/\Gamma_S$ [51]. For the weak interdot coupling, the evolution of $n_{1\sigma}(t)$ is mainly affected by exchanging its electrons with the superconducting lead, whereas in the opposite case (for large V_{12}) both quantum dot occupancies can be partially exchanged. For this reason, $n_{2\sigma}(t)$ remarkably differs from $n_{1\sigma}(t)$ in the limit $\frac{V_{12}}{\Gamma_S} \ll 1$. The term $\sin^2(\bar{s}_1 t)$ appearing in (C10) represents oscillations with the period of $2\pi/(\sqrt{4V_{12}^2 + g_S^2} + g_S)$ and the second term introduces corrections with the period of $4\pi/\Gamma_S$.

The aforementioned initial configuration with only a single electron occupying QD_1 would imply quite different evolution of the considered system in comparison to both quantum dots being initially empty or filled. To illustrate this, we consider here the case when at $t = 0$ the single electron, for instance $\uparrow$, occupies QD_1 (a neighbor of the superconducting lead). The time-dependent occupancies inferred from Eqs. (C4) and (C5) can be rewritten as follows:

$$n_{1\uparrow}(t) = \left\{4V_{12}^2 \sin^2(\Gamma_S t/4) + \Gamma_S^2/4 + V_{12}^2[\cos(\bar{s}_1 t) + \cos(\bar{s}_3 t)]^2\right\}/a^2, \quad \text{(C12)}$$

$$n_{1\downarrow}(t) = V_{12}^2[\cos(\bar{s}_1 t) - \cos(\bar{s}_3 t)]^2/a^2, \quad \text{(C13)}$$

$$n_{2\uparrow}(t) = \left\{4V_{12}^2 \sin^2(\Gamma_S t/4) + \alpha_1 \sin^2(\bar{s}_3 t) + \alpha_3 \sin^2(\bar{s}_1 t) + V_{12}^2[\sin(\bar{s}_1 t) + \sin(\bar{s}_3 t)]^2\right\}/a^2, \quad \text{(C14)}$$

$$n_{2\downarrow}(t) = \left\{\alpha_1 \sin^2(\bar{s}_3 t) + \alpha_3 \sin^2(\bar{s}_1 t) + V_{12}^2[\sin(\bar{s}_1 t) - \sin(\bar{s}_3 t)]^2\right\}/a^2, \quad \text{(C15)}$$

with $a = \sqrt{4V_{12}^2 + g_s^2}$.

Let us consider the case of V_{12} much larger than Γ_S. Performing similar calculations to those done for both QDs initially empty or filled and ignoring the contributions proportional to and smaller than $(\Gamma_S/V_{12})^2$ one obtains

$$n_{1\uparrow}(t) \simeq 1 - \cos^2(\Gamma_S t/4)\sin^2(at/2), \quad \text{(C16)}$$

$$n_{1\downarrow}(t) \simeq \sin^2(\Gamma_S t/4)\sin^2(at/2), \quad \text{(C17)}$$

$$n_{2\uparrow}(t) \simeq 1 - \cos^2(\Gamma_S t/4)\cos^2(at/2) - \frac{x}{8}\sin(\Gamma_S t/2)\sin(at/2), \quad \text{(C18)}$$

$$n_{2\downarrow}(t) \simeq \sin^2(\Gamma_S t/4)\cos^2(at/2) - \frac{x}{8}\sin(\Gamma_S t/2)\sin(at/2). \quad \text{(C19)}$$

Figure 8 shows $n_{1\sigma}(t)$ obtained for $V_{12} = 4\Gamma_S$, where we can clearly identify the quantum oscillations with the period equal to π/V_{12} typical for a two-level system. Their amplitude is modulated with other oscillations, whose period equal to $4\pi/\Gamma_S$ is controlled by the functions $\sin^2(\Gamma_S t/4)$ or $\cos^2(\Gamma_S t/4)$. Let us remark that in the case of a single QD coupled to a superconductor the time-dependent occupancy oscillates with the period twice shorter. Due to electron tunneling between the quantum dots and through the interface between QD_1 and superconducting lead this period of quantum oscillations is present for all types of the initial configurations. Evolution of the second dot occupancy is similar to $n_{1\sigma}(t)$; therefore we skip its presentation.

We now expand the amplitudes of oscillating terms appearing in (C12)–(C15) to the second order in powers of $\frac{1}{x}$:

$$n_{1\uparrow}(t) \simeq 1 - 16x^{-2}\cos^2(\Gamma_S t/4)\sin^2(at/2), \quad \text{(C20)}$$

$$n_{1\downarrow}(t) \simeq 16x^{-2}\sin^2(\Gamma_S t/4)\sin^2(at/2), \quad \text{(C21)}$$

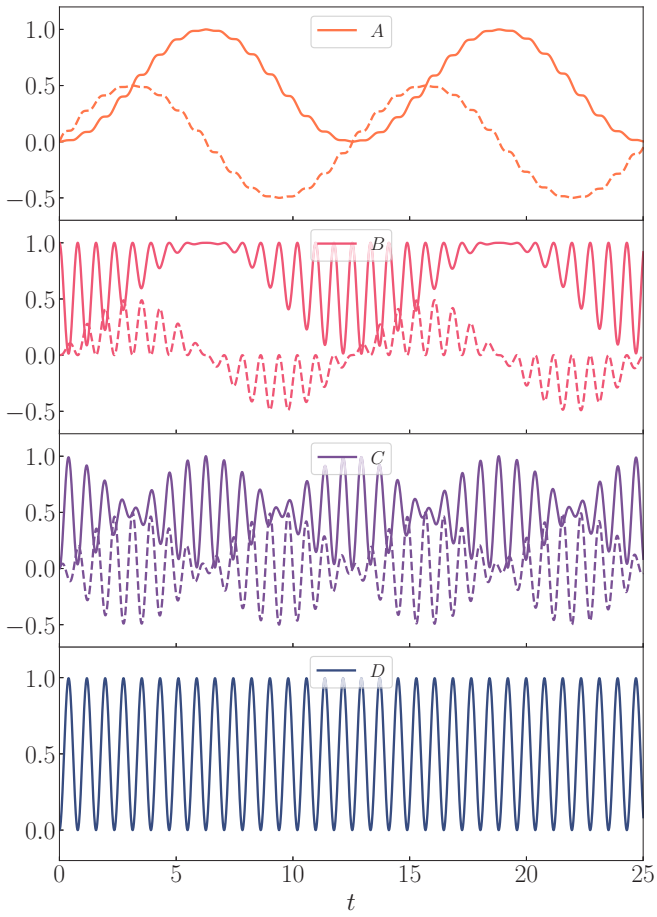

FIG. 10. Time-dependent occupancy $n_{1\uparrow}(t)$ (solid lines) and charge current $j_{S\sigma}(t)$ (dashed curves) obtained for the strong interdot coupling $V_{12} = 4\Gamma_S$ and several initial configurations (QD_2, QD_1): A $= (0, 0)$, B $= (0, \uparrow)$, C $= (\uparrow\downarrow, 0)$, and D $= (\uparrow, \downarrow)$, assuming $\Gamma_S = 1$, $\Gamma_N = 0$, and $\varepsilon_{j\sigma} = 0$.

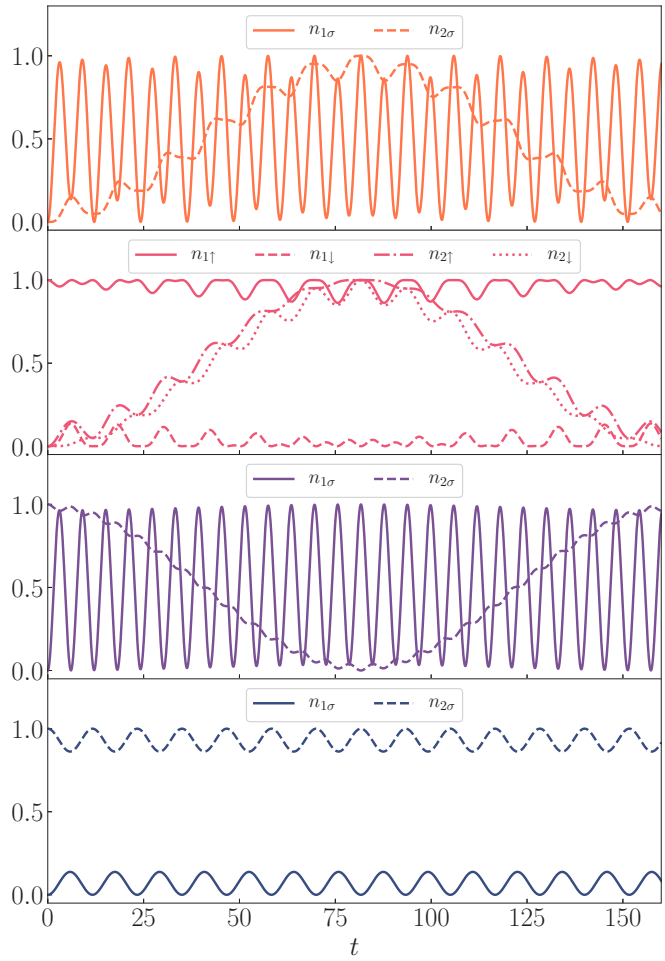

FIG. 11. Time-dependent occupancy $n_{j\sigma}(t)$ (see the legend) obtained for the weak interdot coupling $V_{12} = 0.1\Gamma_S$ and the same initial configuration as in Fig. 10. Other parameters are $\Gamma_S = 1.0$, $\Gamma_N = 0$, $\varepsilon_{j\sigma} = 0$.

$$n_{2\uparrow}(t) \simeq \sin^2(\bar{s}_1 t) + 8y^2[2\sin^2(\Gamma_S t/4) - \sin^2(\bar{s}_1 t) + \sin(\bar{s}_1 t)\sin(\bar{s}_3 t)], \quad \text{(C22)}$$

$$n_{2\downarrow}(t) \simeq \sin^2(\bar{s}_1 t) - 8x^{-2}[\sin^2(\bar{s}_1 t) + \sin(\bar{s}_1 t)\sin(\bar{s}_3 t)]. \quad \text{(C23)}$$

Note that if one neglects all terms proportional to x^{-2} then $n_{1\sigma}(t)$ would not change in time at all, irrespective of its coupling to the second QD. QD_1 is initially singly occupied by the spin-$\uparrow$ electron which, at a later time, might be transferred to QD_2. Such emptying would enable one of the Cooper pairs to leak from the superconducting reservoir onto QD_1 and, in the next step, the spin-$\downarrow$ electron could eventually be transferred onto QD_2. This reasoning explains why $n_{2\downarrow}(t)$ is slowly increasing right after the quench, owing to the terms proportional to x^{-2} in Eq. (C23).

Figure 9 presents $n_{j\sigma}(t)$ obtained for the weak interdot coupling $V_{12} = 0.1\Gamma_S$. Differences between the occupancies of QD_1 and QD_2 are quite evident. QD_1 is nearly completely occupied/empty by $\uparrow/\downarrow$ electrons and such occupancy exhibits oscillations with the period $4\pi/\Gamma_S$ and small amplitude oscillating with another (larger) period $2\pi/(\sqrt{4V_{12}^2 + g_s^2} - g_s)$. Time-dependent $n_{2\sigma}(t)$ is different, because the main contribution in Eqs. (C22) and (C23) simply oscillates with the period equal to $\pi/\bar{s}_1 = 2\pi/(\sqrt{4V_{12}^2 + g_S^2} - g_S)$ and its amplitude is 1. Further corrections, proportional to x^{-2}, introduce small variations of this amplitude, with the period $4\pi/\Gamma_S$.

We have seen that the response of DQD to an abrupt coupling to the superconducting lead strongly depends on the initial fillings $n_{j\sigma}(0)$. It is sufficient to consider four representative types of the initial configurations in order to describe all possible scenarios of the resulting $n_{j\sigma}(t)$ evolution. Figure 10 shows $n_{1\uparrow}(t)$ obtained for the strong interdot coupling $V_{12} = 4\Gamma_S$ for these initial conditions, namely $(QD_2, QD_1) = (0, 0)$, $(0, \uparrow)$, $(\uparrow\downarrow, 0)$, and $(\downarrow, \uparrow)$. Oscillations with the period π/V_{12} are well visible in all curves, whenever at $t = 0$ electrons occupy the QDs. Only for the case of the initially empty dots the oscillations have the period $4\pi/\Gamma_S$ with a small amplitude correction, exhibiting the period π/V_{12}. Specifically for $n_{1\downarrow}(0) = 1 = n_{2\uparrow}(0)$, $n_{1\uparrow}(0) = 0 = n_{2\downarrow}(0)$ [Fig. 10(d)], we

obtain

$$n_{1\uparrow}(t) = \frac{4V_{12}^2}{4V_{12}^2 + g_s^2} \sin^2\left(\frac{\sqrt{4V_{12}^2 + g_s^2}}{2} t\right). \tag{C24}$$

For the large interdot coupling (C24) resembles the Rabi-type oscillations typical for a two-level quantum system.

In the opposite (small V_{12}) case for the initial D configuration we obtain

$$n_{1\uparrow}(t) = 16\frac{V_{12}}{\Gamma_S} \sin^2\left(\frac{\Gamma_S}{4} t\right) \tag{C25}$$

with the period $4\pi/\Gamma_S$ (bottom panel in Fig. 11). For the initial A and B configurations evolution considerably differs from the strong-coupling limit. Notice that the time-dependent occupancies of both QDs are now completely different. The period $2\pi/\Gamma_S$ shows up in $n_{1\sigma}(t)$ for the initial A and C configurations. This period of oscillations can be assigned to the transfer of Cooper pairs back and forth from the superconducting lead onto QD_1. For the other (B and D) cases we observe the oscillations with period $4\pi/\Gamma_S$ in the occupancies of both quantum dots.

For a deeper insight into the transient dynamics of the proximitized DQD we now consider the charge current $j_{S\sigma}(t)$ flowing from the superconducting lead to QD_1 and the interdot current $j_{12\sigma}(t)$, respectively. General expressions for $j_{S\sigma(t)}$ and $j_{12\sigma}(t)$ are presented in Appendix B. Here we focus on their values in the limit $\Gamma_N = 0$:

$$\begin{aligned} j_{S\sigma}(t) = \frac{1}{4V_{12}^2 + g_s^2}\{&2[1 - n_{1\sigma}(0) - n_{1-\sigma}(0)][\bar{s}_1 \sin(\bar{s}_1 t) - \bar{s}_3 \sin(\bar{s}_3 t)][\alpha_1 \cos(\bar{s}_1 t) - \alpha_3 \cos(\bar{s}_3 t)] \\ &+ \Gamma_S V_{12}^2[1 - n_{2\sigma}(0) - n_{2-\sigma}(0)][\cos(\bar{s}_1 t) - \cos(\bar{s}_3 t)][\sin(\bar{s}_1 t) + \sin(\bar{s}_3 t)]\}, \end{aligned} \tag{C26}$$

$$\begin{aligned} j_{12\uparrow/\downarrow}(t) = \frac{2V_{12}^2}{g_s(4V_{12}^2 + g_s^2)}\{&n_{1\uparrow/\downarrow}(0)[\alpha_3 \cos(\bar{s}_3 t) - \alpha_1 \cos(\bar{s}_1 t)][\sin(\bar{s}_1 t) + \sin(\bar{s}_3 t)] \\ &- n_{2\uparrow/\downarrow}(0)[\alpha_3 \cos(\bar{s}_1 t) - \alpha_1 \cos(\bar{s}_3 t)][\sin(\bar{s}_1 t) + \sin(\bar{s}_3 t)] \\ &+ g_s[1 - n_{1\downarrow/\uparrow}(0)][\bar{s}_1 \sin(\bar{s}_1 t) - \bar{s}_3 \sin(\bar{s}_3 t)][\cos(\bar{s}_3 t) - \cos(\bar{s}_1 t)] \\ &+ g_s[1 - n_{2\downarrow/\uparrow}(0)][\bar{s}_1 \sin(\bar{s}_3 t) - \bar{s}_3 \sin(\bar{s}_1 t)][\cos(\bar{s}_3 t) - \cos(\bar{s}_1 t)]\}. \end{aligned} \tag{C27}$$

Broken lines in Fig. 10 display the currents $j_{S\sigma}(t)$ obtained for several initial conditions and the strong interdot coupling, $V_{12} = 4\Gamma_S$. We observe that the time dependence of the current $j_{S\sigma}(t)$ resembles the evolution of $n_{j\uparrow}(t)$, because they are linked through the charge conservation law. In particular, for the initial B and C configurations we recognize the oscillations with period $T \simeq \pi/V_{12}$, which are modulated by the envelope function oscillating with another period $T = 4\pi/\Gamma_S$. Contrary to such behavior, for the initially empty dots the time-dependent current $j_{S\sigma}(t)$ is strictly governed by $\sin^2(\frac{\Gamma_S}{4}t)$ with the period $T = 4\pi/\Gamma_S$.

Equations (C26) and (C27) imply under what initial configuration (QD_2, QD_1) the charge current $j_{S\sigma}(t)$ can eventually vanish. For the case (σ, σ) the charge tunneling is neither allowed to flow from QD_1 to the neighboring QD_2 nor to the superconducting lead, so in consequence the occupancies of DQDs would be frozen. For the other configuration $(\sigma, \bar{\sigma})$ this behavior would not be observed, because the spin-$\downarrow$ (spin-$\uparrow$) electron can tunnel from the first to the second quantum dot simultaneously with the Cooper pair transmittance from the superconducting lead onto QD_1. In the latter case the finite $j_{12\sigma}(t)$ and vanishing $j_{S\sigma}(t)$ currents could be observed.

The initial $(\uparrow, \downarrow)$ or $(\downarrow, \uparrow)$ configurations evolve in time through the intermediate states $(\uparrow\downarrow, 0)$, $(0, \uparrow\downarrow)$, $(\uparrow\downarrow, \uparrow\downarrow)$, $(0, 0)$, $(\uparrow, \downarrow)$, and $(\downarrow, \uparrow)$, respectively. It can be shown, by solving the time-dependent Schrödinger equation, that at arbitrary time the double quantum dot can be found with equal probabilities in the configurations $(0, \uparrow\downarrow)$, $(\uparrow\downarrow, 0)$ or with equal probabilities in the configurations (0,0), $(\uparrow\downarrow, \uparrow\downarrow)$. This means that in both cases the electron pairs can tunnel with the same probability from QD_1 either to the superconducting lead or in the opposite direction. In consequence, the current $j_{S\sigma}(t)$ vanishes. This conclusion can be also formally inferred from Eq. (C26).

For the weak interdot coupling V_{12} and assuming the initial conditions (0,0) or $(\uparrow\downarrow, 0)$, the current $j_{S\sigma}(t)$ evolves with respect to time in a way similar to the occupancy $n_{1\sigma}(t)$ being characterized by the quantum oscillations with period $2\pi/\Gamma_S$ and approximately constant amplitude. For the initial conditions $(0, \uparrow)$ the current $j_{S\sigma}(t)$ oscillates with the period $4\pi/\Gamma_S$, in analogy to time-dependent $n_{1\sigma}(t)$ displayed in Figs. 9 and 11.

We now briefly consider the on-dot $\langle \hat{c}_{j\downarrow}(t)\hat{c}_{j\uparrow}(t)\rangle$ and interdot $\langle \hat{c}_{1\downarrow}(t)\hat{c}_{2\uparrow}(t)\rangle$ pairings, whose general expressions are presented in Appendix B. In the limit of $\Gamma_N = 0$ their simplified analytical expressions are given by

$$\begin{aligned} \langle \hat{c}_{1\downarrow}(t)\hat{c}_{1\uparrow}(t)\rangle = \frac{i}{g_s(4V_{12}^2 + g_s^2)}\{&[1 - n_{1\uparrow}(0) - n_{1\downarrow}(0)][\bar{s}_3 \sin(\bar{s}_3 t) - \bar{s}_1 \sin(\bar{s}_1 t)][\alpha_1 \cos(\bar{s}_1 t) - \alpha_3 \cos(\bar{s}_3 t)] \\ &+ g_s V_{12}^2[1 - n_{2\uparrow}(0) - n_{2\downarrow}(0)][\cos(\bar{s}_3 t) - \cos(\bar{s}_1 t)][\sin(\bar{s}_1 t) + \sin(\bar{s}_3 t)]\}, \end{aligned} \tag{C28}$$

$$\begin{aligned} \langle \hat{c}_{2\downarrow}(t)\hat{c}_{2\uparrow}(t)\rangle = \frac{iV_{12}^2}{4V_{12}^2 + g_s^2}\{&[1 - n_{1\uparrow}(0) - n_{1\downarrow}(0)][\cos(\bar{s}_1 t) - \cos(\bar{s}_3 t)][\sin(\bar{s}_1 t) + \sin(\bar{s}_3 t)] \\ &+ [1 - n_{2\uparrow}(0) - n_{2\downarrow}(0)][\bar{s}_1 \sin(\bar{s}_3 t) - \bar{s}_3 \sin(\bar{s}_1 t)][\bar{s}_3 \cos(\bar{s}_1 t) + \bar{s}_1 \cos(\bar{s}_3 t)]\}/V_{12}^2, \end{aligned} \tag{C29}$$

$$\langle \hat{c}_{1\downarrow}(t)\hat{c}_{2\uparrow}(t)\rangle = \frac{V_{12}}{4V_{12}^2+g_s^2}\{n_{1\uparrow}(0)[\bar{s}_3\sin(\bar{s}_3 t)-\bar{s}_1\sin(\bar{s}_1 t)][\sin(\bar{s}_1 t)+\sin(\bar{s}_3 t)]$$
$$+\frac{1}{g_s}n_{2\uparrow}(0)[\cos(s_1 t)-\cos(s_3 t)][\alpha_1\cos(\bar{s}_3 t)-\alpha_3\cos(\bar{s}_1 t)]$$
$$+\frac{1}{g_s}[1-n_{1\downarrow}(0)][\cos(s_1 t)-\cos(s_3 t)][\alpha_1\cos(\bar{s}_1 t)-\alpha_3\cos(\bar{s}_3 t)]$$
$$+[1-n_{2\downarrow}(0)][\bar{s}_1\sin(\bar{s}_3 t)-\bar{s}_3\sin(\bar{s}_1 t)][\sin(\bar{s}_1 t)+\sin(\bar{s}_3 t)]\}. \quad \text{(C30)}$$

We notice that the on-dot pairing functions (C28) and (C29) are purely imaginary whereas the interdot pairing function (C30) is real. They eventually vanish when each QD is initially singly occupied by the same spin electron. Let us recall that under such circumstances the current $j_{S\sigma}(t)$ vanishes as well. In contrast to this situation, when QDs are initially singly occupied by electrons of opposite spins, then the on-dot pairing functions (C28) and (C29) vanish, whereas the interdot pairing (C30) survives. We have checked that for arbitrary situations the following relationship $j_{S\sigma}(t) = -\Gamma_S \mathrm{Im}\langle \hat{c}_{1\downarrow}(t)\hat{c}_{1\uparrow}(t)\rangle$ is obeyed. This identity has been widely used in studies of the Josephson current under the stationary conditions [65,66].

[1] S. De Franceschi, L. Kouwenhoven, C. Schönenberger, and W. Wernsdorfer, Hybrid superconductor–quantum dot devices, Nat. Nanotechnol. **5**, 703 (2010).

[2] M. S. Kalenkov, A. D. Zaikin, and L. S. Kuzmin, Theory of a Large Thermoelectric Effect in Superconductors Doped with Magnetic Impurities, Phys. Rev. Lett. **109**, 147004 (2012).

[3] L. Hofstetter, S. Csonka, J. Nygård, and C. Schönenberger, Cooper pair splitter realized in a two-quantum-dot Y-junction, Nature (London) **461**, 1476 (2009).

[4] D. Aasen, M. Hell, R. V. Mishmash, A. Higginbotham, J. Danon, M. Leijnse, T. S. Jespersen, J. A. Folk, C. M. Marcus, K. Flensberg, and J. Alicea, Milestones Toward Majorana-Based Quantum Computing, Phys. Rev. X **6**, 031016 (2016).

[5] A. V. Balatsky, I. Vekhter, and J.-X. Zhu, Impurity-induced states in conventional and unconventional superconductors, Rev. Mod. Phys. **78**, 373 (2006).

[6] B. W. Heinrich, J. I. Pascual, and K. J. Franke, Single magnetic adsorbates on *s*-wave superconductors, Prog. Surf. Sci. **93**, 1 (2018).

[7] R. Aguado, Majorana quasiparticles in condensed matter, Riv. Nuovo Cimento **40**, 523 (2017).

[8] R. M. Lutchyn, E. P. A. M. Bakkers, L. P. Kouwenhoven, P. Krogstrup, C. M. Marcus, and Y. Oreg, Majorana zero modes in superconductor-semiconductor heterostructures, Nat. Rev. Mater. **3**, 52 (2018).

[9] G. C. Ménard, S. Guissart, Ch. Brun, R. T. Leriche, M. Trif, F. Debontridder, D. Demaille, D. Roditchev, P. Simon, and T. Cren, Two-dimensional topological superconductivity in Pb/Co/Si(111), Nat. Commun. **8**, 2040 (2017).

[10] W. G. van der Wiel, S. De Franceschi, J. M. Elzerman, T. Fujisawa, S. Tarucha, and L. P. Kouwenhoven, Electron transport through double quantum dots, Rev. Mod. Phys. **75**, 1 (2002).

[11] K. C. Nowack, F. H. L. Koppens, Yu. V. Nazarov, and L. M. K. Vandersypen, Coherent control of a single electron spin with electric fields, Science **318**, 1430 (2007).

[12] D. Sherman, J. S. Yodh, S. M. Albrecht, J. Nygård, P. Krogstrup, and C. M. Marcus, Normal, superconducting and topological regimes of hybrid double quantum dots, Nat. Nanotechnol. **12**, 212 (2017).

[13] K. Grove-Rasmussen, G. Steffensen, A. Jellinggaard, M. H. Madsen, R. Žitko, J. Paaske, and J. Nygård, Yu-Shiba-Rusinov screening of spins in double quantum dots, Nat. Commun. **9**, 2376 (2018).

[14] J. C. Estrada Saldaña, A. Vekris, G. Steffensen, R. Žitko, P. Krogstrup, J. Paaske, K. Grove-Rasmussen, and J. Nygård, Supercurrent in a Double Quantum Dot, Phys. Rev. Lett. **121**, 257701 (2018).

[15] J. C. Estrada Saldaña, A. Vekris, R. Žitko, G. Steffensen, P. Krogstrup, J. Paaske, K. Grove-Rasmussen, and J. Nygård, Two-impurity Yu-Shiba-Rusinov states in coupled quantum dots, Phys. Rev. B **102**, 195143 (2020).

[16] D. Bouman, R. J. J. van Gulik, G. Steffensen, D. Pataki, P. Boross, P. Krogstrup, J. Nygård, J. Paaske, A. Pályi, and A. Geresdi, Triplet-blockaded Josephson supercurrent in double quantum dots, Phys. Rev. B **102**, 220505(R) (2020).

[17] P. Zhang, H. Wu, J. Chen, S. A. Khan, P. Krogstrup, D. Pekker, and S. M. Frolov, Evidence of Andreev blockade in a double quantum dot coupled to a superconductor, arXiv:2102.03283.

[18] Z. Su, A. B. Tacla, M. Hocevar, D. Car, S. R. Plissard, E. P. A. M. Bakkers, A. J. Daley, D. Pekker, and S. M. Frolov, Andreev molecules in semiconductor nanowire double quantum dots, Nat. Commun. **8**, 585 (2017).

[19] A. Zarassi, Z. Su, J. Danon, J. Schwenderling, M. Hocevar, B. M. Nguyen, J. Yoo, S. A. Dayeh, and S. M. Frolov, Magnetic field evolution of spin blockade in Ge/Si nanowire double quantum dots, Phys. Rev. B **95**, 155416 (2017).

[20] J.-P. Cleuziou, W. Wernsdorfer, V. Bouchiat, T. Ondarcuhu, and M. Monthioux, Carbon nanotube superconducting quantum interference device, Nat. Nanotechnol. **1**, 53 (2006).

[21] J.-D. Pillet, P. Joyez, R. Žitko, and M. F. Goffman, Tunneling spectroscopy of a single quantum dot coupled to a superconductor: From Kondo ridge to Andreev bound states, Phys. Rev. B **88**, 045101 (2013).

[22] M. Ruby, B. W. Heinrich, Y. Peng, F. von Oppen, and K. J. Franke, Wave-Function Hybridization in Yu-Shiba-Rusinov Dimers, Phys. Rev. Lett. **120**, 156803 (2018).

[23] D.-J. Choi, C. G. Fernández, E. Herrera, C. Rubio-Verdú, M. M. Ugeda, I. Guillamón, H. Suderow, J. I. Pascual, and N. Lorente, Influence of Magnetic Ordering between Cr Adatoms on the

Yu-Shiba-Rusinov States of the β-Bi_2Pd Superconductor, Phys. Rev. Lett. **120**, 167001 (2018).

[24] S. Kezilebieke, R. Žitko, M. Dvorak, and P. Liljeroth, Observation of coexistence of Yu-Shiba-Rusinov states and spin-flip excitations, Nano Lett. **19**, 4614 (2019).

[25] F. Küster, A. M. Montero, F. S. M. Guimaraes, S. Brinker, S. Lounis, S. S. P. Parkin, and P. Sessi, Correlating Josephson supercurrents and Shiba states in quantum spins unconventionally coupled to superconductors, Nat. Commun. **12**, 1108 (2021).

[26] M.-S. Choi, C. Bruder, and D. Loss, Spin-dependent Josephson current through double quantum dots and measurement of entangled electron states, Phys. Rev. B **62**, 13569 (2000).

[27] Y. Zhu, Q.-F. Sun, and T.-H. Lin, Probing spin states of coupled quantum dots by a dc Josephson current, Phys. Rev. B **66**, 085306 (2002).

[28] Y. Tanaka, N. Kawakami, and A. Oguri, Correlated electron transport through double quantum dots coupled to normal and superconducting leads, Phys. Rev. B **81**, 075404 (2010).

[29] R. Žitko, M. Lee, R. López, R. Aguado, and M.-S. Choi, Josephson Current in Strongly Correlated Double Quantum Dots, Phys. Rev. Lett. **105**, 116803 (2010).

[30] J. Eldridge, M. G. Pala, M. Governale, and J. König, Superconducting proximity effect in interacting double-dot systems, Phys. Rev. B **82**, 184507 (2010).

[31] A. Martín-Rodero and A. Levy Yeyati, Josephson and Andreev transport through quantum dots, Adv. Phys. **60**, 899 (2011).

[32] S. Droste, S. Andergassen, and J. Splettstoesser, Josephson current through interacting double quantum dots with spin–orbit coupling, J. Phys.: Condens. Matter **24**, 415301 (2012).

[33] S. Pfaller, A. Donarini, and M. Grifoni, Subgap features due to quasiparticle tunneling in quantum dots coupled to superconducting leads, Phys. Rev. B **87**, 155439 (2013).

[34] A. Brunetti, A. Zazunov, A. Kundu, and R. Egger, Anomalous Josephson current, incipient time-reversal symmetry breaking, and Majorana bound states in interacting multilevel dots, Phys. Rev. B **88**, 144515 (2013).

[35] N. Y. Yao, C. P. Moca, I. Weymann, J. D. Sau, M. D. Lukin, E. A. Demler, and G. Zaránd, Phase diagram and excitations of a Shiba molecule, Phys. Rev. B **90**, 241108(R) (2014).

[36] B. Sothmann, S. Weiss, M. Governale, and J. König, Unconventional superconductivity in double quantum dots, Phys. Rev. B **90**, 220501(R) (2014).

[37] P. Trocha and I. Weymann, Spin-resolved Andreev transport through double-quantum-dot Cooper pair splitters, Phys. Rev. B **91**, 235424 (2015).

[38] T. Meng, J. Klinovaja, S. Hoffman, P. Simon, and D. Loss, Superconducting gap renormalization around two magnetic impurities: From Shiba to Andreev bound states, Phys. Rev. B **92**, 064503 (2015).

[39] R. Žitko, Numerical subgap spectroscopy of double quantum dots coupled to superconductors, Phys. Rev. B **91**, 165116 (2015).

[40] K. Wrześniewski and I. Weymann, Kondo physics in double quantum dot based Cooper pair splitters, Phys. Rev. B **96**, 195409 (2017).

[41] A. Ptok, S. Głodzik, and T. Domański, Yu-Shiba-Rusinov states of impurities in a triangular lattice of $NbSe_2$ with spin-orbit coupling, Phys. Rev. B **96**, 184425 (2017).

[42] D. Pekker and S. M. Frolov, Andreev blockade in a double quantum dot with a superconducting lead, arXiv:1810.05112.

[43] Z. Scherübl, A. Pályi, and S. Csonka, Transport signatures of an Andreev molecule in a quantum dot-superconductor-quantum dot setup, Beilstein J. Nanotechnol. **10**, 363 (2019).

[44] K. P. Wójcik and I. Weymann, Nonlocal pairing as a source of spin exchange and Kondo screening, Phys. Rev. B **99**, 045120 (2019).

[45] V. Pokorný, M. Žonda, G. Loukeris, and T. Novotný, Second order perturbation theory for a superconducting double quantum dot, JPS Conf. Proc. **30**, 011002 (2020).

[46] X.-Q. Wang, S.-F. Zhang, Y. Han, and W.-J. Gong, Fano-Andreev effect in a parallel double quantum dot structure, Phys. Rev. B **100**, 115405 (2019).

[47] Z.-Z. Li and M. Leijnse, Quantum interference in transport through almost symmetric double quantum dots, Phys. Rev. B **99**, 125406 (2019).

[48] K. G. Wilson, The renormalization group: Critical phenomena and the Kondo problem, Rev. Mod. Phys. **47**, 773 (1975).

[49] F. B. Anders and A. Schiller, Real-Time Dynamics in Quantum-Impurity Systems: A Time-Dependent Numerical Renormalization-Group Approach, Phys. Rev. Lett. **95**, 196801 (2005).

[50] R. Bulla, T. A. Costi, and T. Pruschke, Numerical renormalization group method for quantum impurity systems, Rev. Mod. Phys. **80**, 395 (2008).

[51] R. Taranko and T. Domański, Buildup and transient oscillations of Andreev quasiparticles, Phys. Rev. B **98**, 075420 (2018).

[52] R. Taranko, T. Kwapiński, and T. Domański, Transient dynamics of a quantum dot embedded between two superconducting leads and a metallic reservoir, Phys. Rev. B **99**, 165419 (2019).

[53] T. L. Schmidt, P. Werner, L. Mühlbacher, and A. Komnik, Transient dynamics of the Anderson impurity model out of equilibrium, Phys. Rev. B **78**, 235110 (2008).

[54] R. S. Souto, A. Martín-Rodero, and A. Levy Yeyati, Quench dynamics in superconducting nanojunctions: Metastability and dynamical Yang-Lee zeros, Phys. Rev. B **96**, 165444 (2017).

[55] R. Seoane Souto, R. Avriller, A. Levy Yeyati, and A. Martín-Rodero, Transient dynamics in interacting nanojunctions within self-consistent perturbation theory, New J. Phys. **20**, 083039 (2018).

[56] F. B. Anders and A. Schiller, Spin precession and real-time dynamics in the Kondo model: Time-dependent numerical renormalization-group study, Phys. Rev. B **74**, 245113 (2006).

[57] H. T. M. Nghiem and T. A. Costi, Time-dependent numerical renormalization group method for multiple quenches: Application to general pulses and periodic driving, Phys. Rev. B **90**, 035129 (2014).

[58] H. T. M. Nghiem and T. A. Costi, Generalization of the time-dependent numerical renormalization group method to finite temperatures and general pulses, Phys. Rev. B **89**, 075118 (2014).

[59] We used the open-access Budapest Flexible DM-NRG code, http://www.phy.bme.hu/~dmnrg; O. Legeza, C. P. Moca, A. I. Tóth, I. Weymann, and G. Zaránd, arXiv:0809.3143.

[60] A. Weichselbaum and J. von Delft, Sum-Rule Conserving Spectral Functions from the Numerical Renormalization Group, Phys. Rev. Lett. **99**, 076402 (2007).

[61] A. Weichselbaum, Tensor networks and the numerical renormalization group, Phys. Rev. B **86**, 245124 (2012).

[62] K. Wrześniewski and I. Weymann, Quench dynamics of spin in quantum dots coupled to spin-polarized leads, Phys. Rev. B **100**, 035404 (2019).

[63] E. Prada, P. San-Jose, M. W. A. de Moor, A. Geresdi, E. J. H. Lee, J. Klinovaja, D. Loss, J. Nygård, R. Aguado, and L. P. Kouwenhoven, From Andreev to Majorana bound states in hybrid superconductor-semiconductor nanowires, Nat. Rev. Phys. **2**, 575 (2020).

[64] R. Aguado, A perspective on semiconductor-based superconducting qubits, Appl. Phys. Lett. **117**, 240501 (2020).

[65] M. Žonda, V. Pokorný, V. Janiš, and T Novotný, Perturbation theory of a superconducting 0-π impurity quantum phase transition, Sci. Rep. **5**, 8821 (2015).

[66] T. Domański, M. Žonda, V. Pokorný, G. Górski, V. Janiš, and T. Novotný, Josephson-phase-controlled interplay between correlation effects and electron pairing in a three-terminal nanostructure, Phys. Rev. B **95**, 045104 (2017).